

THE DYNAMICS OF LAVA FLOWS

R. W. Griffiths

*Research School of Earth Sciences, The Australian National University, Canberra,
Australia; 0200 ACT*

Key Words emplacement dynamics, rheology, gravity currents, viscous flow, Bingham fluids, cooling, solidification, melting

■ **Abstract** Lava flows are gravity currents of partially molten rock that cool as they flow, in some cases melting the surface over which they flow but in all cases gradually solidifying until they come to rest. They present a wide range of flow regimes from turbulent channel flows at moderate Reynolds numbers to extremely viscous or plastic, creeping flows, and even brittle rheology may play a role once some solid has formed. The cooling is governed by the coupling of heat transport in the flowing lava with transfer from the lava surface into the surrounding atmosphere or water or into the underlying solid, and it leads to large changes in rheology. Instabilities, mostly resulting from cooling, lead to flow branching, surface folding, rifting, and fracturing, and they contribute to the distinctive styles and surface appearances of different classes of flows. Theoretical and laboratory models have complemented field studies in developing the current understanding of lava flows, motivated by the extensive roles they play in the development of planetary crusts and ore deposits and by the immediate hazards posed to people and property. However, much remains to be learned about the mechanics governing creeping, turbulent, and transitional flows in the presence of large rheology change on cooling and particularly about the advance of flow fronts, flow instabilities, and the development of flow morphology. I introduce the dynamical problems involved in the study of lava flows and review modeling approaches.

1. INTRODUCTION

Lava flows form when molten or partially molten rock is erupted onto the surface of Earth or other rocky planets. Eruptions are forced by buoyancy caused by density differences between the melt and surrounding rock and by the pressures generated by exsolution of volatiles. The melt spreads on the surface as a gravity current, forming a lava flow. The lava is not a simple liquid but generally a mix of silicate liquid, crystals, and gas bubbles, with additional increases in crystal and bubble fractions during the evolution of the flow. Surface heat fluxes from the lava are generally large enough to cause rapid quenching of a thin surface layer to an amorphous glassy solid, and the slower process of crystallization leads eventually to complete solidification of the flow. The behavior of lava flows, their

structure, rate of flow frontal advance, and instabilities vary depending on the properties of the erupted magma, the effusion rate, the ground topography over which the lava flows, and its new environment (which primarily determines the rate of heat loss). The flow front eventually comes to a halt, in some cases before the vent supply shuts off.

Although this review focuses on theoretical and experimental studies of flow dynamics, it is worthwhile briefly outlining for the interested fluid mechanician some of the motivation for and broader background to such studies. These naturally include a desire to assess the direct hazards posed to people and property by advancing lava flows, a recurring threat of frequently erupting volcanoes such as Etna, in Sicily, and Kilauea, in Hawaii, and by the much more destructive forces of pyroclastic flows, which give less warning, as at Merapi, in Indonesia, in 1994, and during the eruption of Unzen, in Japan, in 1991–1995. Lava also melts snowcaps, as at Redoubt Volcano, in Alaska, in 1989, and can lead to flash floods and mud flows. These hazards depend on such factors as the rheology of the lava, its effusion rate, the existing ground topography, the distance the flow front advances before it solidifies, and the steepness and stability of lava domes. A further motivation to understand lava flow dynamics is the interpretation of observations of ancient or remote flows, in which the flow shape, structure, and surface features (its morphology) can hold clues to the eruption rates and lava rheology. For extraterrestrial flows, estimates of the rheology and eruption rates have already been made, based on flow morphology. These, in turn, are used to infer chemical composition of the magmas and the nature of the tectonic mechanisms responsible for the volcanism. In submarine flows, lava composition can be obtained by direct measurement, but the eruptions are rarely observed during their active phase, and so information on eruption rates might again be obtained from the form of the solidified flows. Other aims of lava flow modeling are to understand the formation of nickel-iron-copper sulfide ore deposits from ancient high-temperature (komatiite) flows and the emplacement of particularly remarkable surface features, such as very large rhyolite flows on Earth, large “pancake” domes observed on the surface of Venus, and basalt flows over 100 km long on Earth, the Moon, and Mars.

In the modeling of lava flows, both process-oriented models and the computational-simulation approach have a useful role, although particular care must be taken to ensure that the formulations of complicated numerical models have a sound physical basis. Simplified isothermal models of low-Reynolds-number and viscoplastic flows have demonstrated the way in which slow eruptions of lava would advance in the absence of cooling, and recently these have provided the basis for models that include heterogeneous rheology and rheological change caused by cooling and solidification. Results from models of melting of the underlying base and erosion by turbulent lavas are providing an improved basis for understanding contamination of the lava by the underlying rocks and the deposition of metal ores. Laboratory analog models have provided tests for the simplest of flow models, as well as a means of exploring a range of instabilities

and complex flow regimes that have not yet been addressed by theoretical or computational models.

In this review I focus on the flow of lava on the surface (neglecting the equally interesting dynamics beneath the surface, which force the eruption of magma). In Section 2, I provide further background to the fluid-dynamical problems by briefly summarizing the observed range of styles of lava flows. In Sections 3 and 4, I introduce the physical properties of lavas and the nature of the surface heat fluxes, both of which determine the rates at which the lavas cool, increase in viscosity, and solidify. The range of dynamical-flow regimes is discussed in Section 5, along with results from isothermal models of extremely viscous and plastic flows. In Section 6, we turn to the role of thermal effects, particularly solidification at the free surface in both creeping flows and long lava flows, and of thermal erosion of underlying ground in turbulent flows. Concluding comments on progress toward understanding lava flows and the challenge ahead are given in Section 7. The review includes some references to observational work, field data, and laboratory experiments on the properties of lava samples. However, there is no intent to be complete in these areas, because a review of observations would require far more space than is available here, and the purpose is to focus on theoretical and experimental studies of the relevant dynamics.

2. OBSERVED STYLES OF FLOW

There are a number of styles of lava flow, each presumably reflecting a different dynamical regime. Some examples are shown in Figure 1. The style of flow is related, through lava composition, eruption temperature, and effusion rate, to the class of volcano. On some volcanoes the effusion of melt is the dominant form of activity, whereas explosive eruptions are common in other cases. Lava flows are generally dominant for basaltic volcanism at volcanic “hotspots” (notably oceanic-island chains, of which Hawaii and Iceland are examples) and at mid-ocean ridges (where the seafloor plates are moving apart, causing the underlying mantle to upwell and undergo small degrees of partial melting, giving rise to a more-or-less continuous supply of mid-ocean ridge basalts). In these cases the lavas, at their vents, are among the hottest and least viscous on Earth today. Their effusion rates can also be large, producing rapid channelized flows that may be turbulent and travel for long distances. Ancient eruptions of even hotter and less viscous lavas called komatiites [generally thought to originate from hotspots in the Archaean and proterozoic eras, $> 2 \times 10^9$ years ago (e.g. Huppert et al 1984, Williams et al 1998)], and enormous outpourings of flood basalts, which flowed hundreds of kilometers (e.g. see review by Cashman et al 1998) and generated large plateaus on both continents and ocean floors, have been preserved in regions of the Earth’s crust. These testify to flows much faster and more turbulent than any historically recorded.

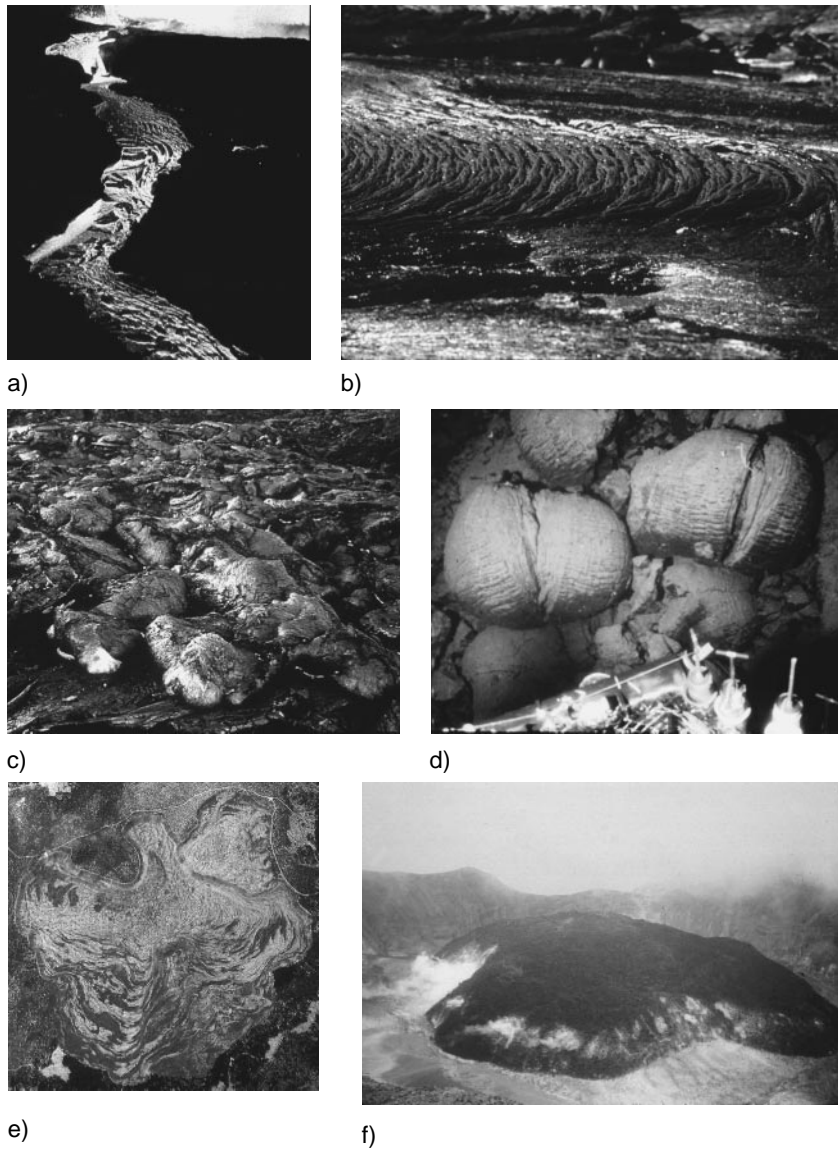


Figure 1 Examples of some lava flow forms. (a) Channelized basalt flow from Kilauea Volcano, Hawaii (flow channel ~ 20 m wide); (b) and (c) “ropy pahoehoe” and “toey pahoehoe,” respectively, from Kilauea (“ropes” have wavelength ~ 20 cm; “toes” are typically 30 cm across); (d) submarine-pillow basalts, each ~ 1 m across, on the East Pacific Rise; (e) Little Glass Mountain rhyolite flow, northern California, showing flow around an obstacle on a gentle slope and transverse surface ridges of ~ 5 m in height (image 2.8 km across); (f) a lava dome 850 m across and 130 m high in the crater of La Soufrière, St. Vincent, 1979. Photographs courtesy of JH Fink & R Embley.

The largest of present-day flows are those of Hawaii, which often commence their journey on the mountain slopes as rapid, open-channel “pahoehoe” flows (Figure 1a). They commonly change their form some kilometers from the vent to become slowly creeping flows (called “a`a”) with a capping of solid blocks and a thick (≤ 10 -m) flow front (e.g. Kilburn 1993, Cashman et al 1999b). In both forms they produce their own channel by construction of levees of solidified lava (Hulme 1974). Outbreaks from a channel or flow front can tap the hot interior fluid and commonly produce shallow flows with thin glassy surfaces (also called “pahoehoe” lava). Some of these flows advance with smooth surfaces, others with their surface folded into a “ropy” appearance (Figure 1b), others in toelike protrusions (Figure 1c). Rapid channel flows can also form lava tubes, which are roofed channels in which the flowing melt is completely surrounded by solidified lava and therefore well insulated against surface heat loss (Kauahikaua et al 1998). Submarine mid-ocean ridge eruptions of basalt, although of similar viscosity, are often much slower, and the Reynolds number can be small. These types of lava are also much more rapidly cooled by the water. Slow submarine eruptions give rise to fields of “pillow basalts” (Figure 1d), each composed of a slowly spreading mound of meter-sized lobes (Moore 1975). “Pillow” morphology is known to have occurred even in ancient high-temperature komatiite flows now exposed in Western Australia.

At volcanoes found above the scene of active subduction of the sea floor (e.g. western North America, Indonesia, the Philippines, and Japan), lavas have lower temperatures and much greater apparent viscosity. In these cases a relatively slow effusion of lava is sometimes sustained for months or years (often between explosive eruptions), and the resulting flows have extremely low Reynolds numbers. Examples are large rhyolite flows (Figure 1e) and 100-m- to 1-km-sized mounds referred to as lava domes, the most viscous of which tend to grow slowly over months or years (Figure 1f). These domes have a solid surface layer but remain mobile for days to months, with the solid undergoing plastic or brittle deformation (Anderson & Fink 1990). On occasions, a section of a lava dome may collapse down the mountain slope either as a block-and-ash flow or, if there is an explosive release of pressure, as a destructive pyroclastic flow. Domes show obvious non-Newtonian behavior (Anderson & Fink 1990, Fink et al 1990, Fink & Griffiths 1998), including fractures (or “creases”) in the vent region at which the lava slowly opens and diverges as it is extruded, smooth extrusion surfaces where one part of the lava slid past another, and tall angular spines.

3. LAVA RHEOLOGY

The rheology of lava as it is erupted from a vent depends on composition, temperature, crystal content, and bubble content. It is therefore time dependent as a result of cooling, crystallization, and vesiculation. If the lava is viewed as a viscous fluid, four different shear viscosity coefficients can be defined: the melt

viscosity η_m of the liquid phase alone; the (actual) lava viscosity η ($= d\sigma/d\dot{\epsilon}$, where σ is the applied shearing stress, and $\dot{\epsilon}$ is the strain rate) of the liquid-crystal-bubble mixture that makes up the lava; the apparent lava viscosity η_A ($= \sigma/\dot{\epsilon}$) of this mixture; and an apparent flow viscosity η_F that is an effective viscosity for a whole lava flow and which, in some way, averages over potentially large differences in η and η_A from place to place within the flow (and over time if desired). The melt viscosity governs the microphysics of the growth, migration, coalescence, and deformation of bubbles (Manga & Stone 1994, Manga et al 1998). It is identical to the actual lava rheology for small crystal and bubble fractions. It is temperature dependent but likely to be close to Newtonian. Both the actual and apparent lava viscosities, η and η_A , on the other hand, are a result of the microphysics of the liquid-crystal-bubble mixture and are the relevant macroscopic viscosities governing the flow. Lava flows have wide-ranging crystal contents at the vent (from $<5\%$ in many basalts and rhyolites to commonly 30% – 50% for andesite and dacites), and these increase with distance from the vent (Figure 2a). Bubbles typically occupy anything from a few percent by volume to $>90\%$ in highly vesiculated portions of a flow (see electron micrographs of Cashman et al 1999a; Figure 2b). The actual and apparent viscosities will in general differ as a result of a finite yield stress or a nonlinear relation between shearing stress and strain rate. Use of an apparent flow viscosity η_F ignores the actual

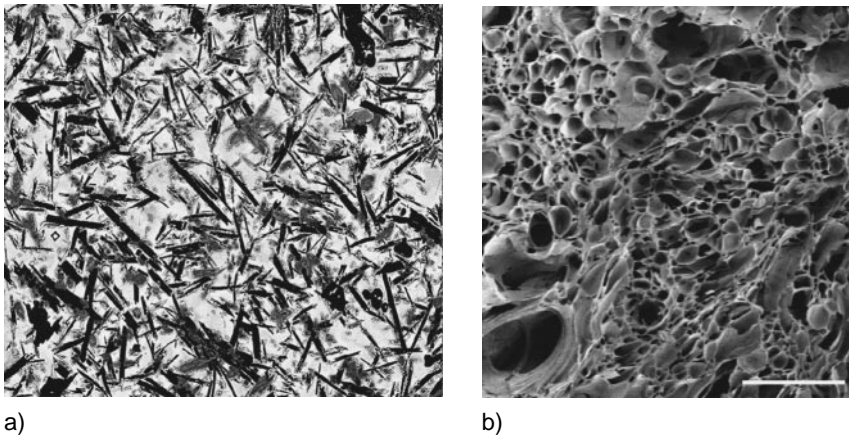


Figure 2 Images of (a) crystallinity in an α sample taken from an active lava channel 2 km from its vent on Kilauea Volcano, Hawaii, in 1997, and thought to be responsible for a yield strength (this back-scattered electron micrograph shows an area of ~ 0.4 mm across and a crystal volume fraction of $\sim 45\%$ (Cashman et al 1999b); and (b) vesiculation in a common form of pumice produced by pyroclastic eruptions (this scanning electron micrograph shows an area of ~ 0.5 mm across; sample from Mt. Mazama, USA (Cashman et al 1999a). Additional fascinating images indicating changing crystallinity and effects of shear on vesicles are to be seen in these references.

nature of the rheology and is used to characterize the whole of a thermally and rheologically heterogeneous flow in terms of a single rheological variable. It therefore represents little of the actual mechanics of flow.

An approximation that is sometimes used to describe lava rheology is the Bingham flow law (Shaw et al 1968, Shaw 1969, Murase & McBirney 1973, Hulme 1974, McBirney & Murase 1984), in which the shearing stress σ and strain rate $\dot{\epsilon}$ are related by

$$\sigma = \sigma_0 + \eta \dot{\epsilon}, \quad (1)$$

where σ_0 is the yield stress and η is a constant viscosity (referred to as the plastic viscosity). When the applied stress is below the yield stress, there is no deformation [other than brittle or elastic, which are neglected here (Nguyen & Boger 1992)], but once this limit is exceeded, the flow may be characterized by an apparent viscosity $\eta_A = \eta + \sigma_0/\dot{\epsilon}$. Thus, for small strain rates, the yield stress can give rise to an apparent viscosity that is very much greater than the actual viscosity. We neglect elastic deformation because the important length scale of shearing in lava flows is small (on the order of the flow depth) and because, on all but small pahoehoe flows, the solid parts are observed to be highly fractured. The fracturing is a result of brittle failure under thermal and flow stresses and tends to produce a carapace of plates, blocks, or rubble.

The viscosity of lava is a function of the temperature T , the volume fraction of crystals ϕ , and, to a lesser extent, the size and shape of the crystals. Thus a single relation is not likely to be accurate for a range of lava types having different compositions, temperatures, and histories. However, for basaltic lavas the apparent viscosity is often taken to follow the Einstein-Roscoe relation (Roscoe 1952, 1953; Marsh 1981; Pinkerton & Stevenson 1992)

$$\eta_A(T, \phi) = \eta_0 (1 - \phi/\phi_{\max})^{-2.5} e^{\gamma(T_0 - T)}, \quad (2)$$

where ϕ_{\max} is the maximum crystal fraction that will allow flow, γ is a constant [$\gamma \approx 0.04$ (Dragoni 1989)], and T_0 and η_0 are reference values (such as those at the vent). Highly silicic magma has greater melt viscosity by virtue of its composition and generally cooler temperature. It might or might not have higher crystallinity, depending on water content, because the crystal fraction ϕ is related to the temperature and composition of the lava. One approach might be to model the crystallinity of basaltic magmas by

$$\phi(x) = \phi_0 + \phi_f (T_0 - T)/(T_0 - T_{sol}), \quad (3)$$

where ϕ_0 is the initial (vent) crystal fraction, ϕ_f is the total further amount of crystallization that occurs during flow, and T_{sol} is the solidus temperature. Here $\phi_0 + \phi_f \leq 1$. An alternative is to use an effective solidification temperature and $\phi_0 + \phi_f = \phi_{\max}$ in Equation 3.

Equation 2 illustrates the expectation that all lavas reach a limit of extremely large apparent viscosity caused by the onset of a yield stress for a critical crystal content ϕ_{\max} . Early experimental evidence suggested that $\phi_{\max} \approx 0.55$ – 0.6 for

silicate melts (Marsh 1981). More recent results confirm that the use of this value in Equation 2 is appropriate (Lejeune & Richet 1995), although the latter results also show the onset of non-Newtonian behavior for $\phi_{\max} \approx 0.4$ (at which $\eta_A > 10^9$ Pas, and yield stress is on the order of 2×10^6 Pa). Independent evidence from Hawaiian samples indicates that basalt flows become controlled by a yield strength at $\phi \approx 45\%–50\%$ (Cashman et al 1999b; Figure 2a). These are the crystal contents at which the relative motion of the crystals begins to be inhibited by their overlapping and interlocking (Kerr & Lister 1991). In situ instrumental measurements of the yield strength for basalts on Mt. Etna have given values of 400–6000 Pas [(Pinkerton & Sparks 1978)].

The effects of bubbles on lava rheology are less well understood but will generally be less important than crystals (Manga et al 1998). Very small bubbles are effectively rigid under surface tension forces and can increase the viscosity. Larger bubbles, on the other hand, deform in shear, providing slippage and leading to shear-thinning behavior (Cashman et al 1999a, Manga & Stone 1994). A similar response may occur if elongated crystals become aligned with the shear. Such shear-thinning behavior can be modeled by using a simple power-law stress-strain rate relation or the Herschel-Bulkley generalization of the Bingham rheology (Huang & Garcia 1998, Balmforth et al 1999):

$$\begin{aligned}\phi_{ij} &= (K\dot{\epsilon}^{n-1} + \sigma_0/\dot{\epsilon})\epsilon_{ij} \quad \text{for } \sigma > \sigma_0, \\ \epsilon_{ij} &= 0 \quad \text{for } \sigma \leq \sigma_0,\end{aligned}\tag{4}$$

where σ_{ij} are the deviatoric stresses, $\sigma = \sqrt{(1/2) \sigma_{jk}\sigma_{jk}}$, ϵ_{ij} are elements of the rate of strain tensor, $\dot{\epsilon} = \sqrt{(1/2) \epsilon_{jk}\epsilon_{jk}}$ is the shear rate, K is the consistency (a measure of the resistance to shear), n is an index characterizing the nonlinearity, and σ_0 is again the yield stress. For $n = 1$, we have a Bingham fluid in which the deviatoric stresses are proportional to the shear rate and $K = \eta$, the plastic viscosity. When $n < 1$, shear leads to reduction of the applied stress required to achieve that shear rate (as in shear-thinning, vesicle-rich lava), whereas, if $n > 1$, as suggested by Smith (1997) for crystal-rich lava near the solidus, the fluid would be shear thickening.

Given the range of influences on lava rheology, it is not surprising that lava flows can be heterogeneous. Heterogeneity within a flow occurs owing to cooling, crystallization or exsolution of volatiles during flow, or a change in magma properties when a stratified magma chamber is progressively tapped during an eruption. All of these causes can be important. Cooling, in particular and as we will see in Section 6, leads to a very complex surface layer that may subsequently inhibit flow of the hotter lava of the flow interior. The surface layer consists largely of glassy lava formed by rapid cooling to the glass transition temperature of $\sim 700^\circ\text{C}$, as well as, presumably, some cooled but not yet solidified underlying lava. This layer might be viewed as a more viscous one (Huppert et al 1982, Stasiuk et al 1993) or an elastic shell having a tensile strength (Iverson 1990). However, it seems more likely that the highly fractured and blocky carapace on

large flows might be better described by either an internal friction coefficient (a Coulomb rheology, assuming a 'dry' blocky layer, as in the flow of sand) or a yield stress for shearing motion that will eventually bring the flow to a halt (Hulme 1974, Griffiths & Fink 1993).

4. LAVA TEMPERATURES AND COOLING MECHANISMS

Lava is erupted onto the surface with temperatures and viscosities that largely relate to its composition. The hottest lava (komatiite, with low silica and high magnesium content) has had eruption temperatures of 1400–1600°C. The basaltic lava at volcanic hotspots such as Hawaii emerges at $\leq 1200^\circ\text{C}$, and mid-ocean ridge basalts erupt at 1100°C . These basalts have viscosities $\eta_A \approx \eta \sim 10^2\text{--}10^3$ Pas on eruption and have no significant yield stress before cooling and crystallization occur (McBirney & Murase 1984). At the other end of the scale are the relatively silicic and more viscous types of magma (andesite and dacite) erupted at around 900°C above zones of lithosphere subduction and caused by melting of a fraction of the down-going lithosphere. These types of magma have $\eta_A \sim 10^5\text{--}10^8$ Pas (a value not to be confused with the apparent flow viscosity η_F , which for one dome is estimated to be on the order of 10^{11} Pas; Huppert et al 1982).

When lava is extruded with eruption temperature T_e into an environment at ambient temperature T_a , the temperature difference $\Delta T = T_e - T_a$ implies a surface heat flux $F_s(t)$, the magnitude of which depends on the heat transfer mechanisms on each side of the surface. The surface flux and surface (or contact) temperature $T_c(t)$ are strongly coupled, each adjusting to the other and to heat transfer within the lava. The contact temperature is generally much less than the interior temperature of the lava, and both T_c and F_s can be estimated by matching the heat fluxes on both sides of the surface (Griffiths & Fink 1992a,b; Neri 1998; Williams et al 1998). Heat loss from the surface is caused by radiation and convection. Heat transport within the lava is discussed in Section 6.

The radiative flux F_R from the surface is readily calculated as a function of T_c from Stefan's law: $F_R = e\Sigma(T_c^4 - T_a^4)$, where e is the surface emissivity (generally $e > 0.9$), Σ is the Stefan-Boltzmann constant, and T_a is the ambient temperature. The convective heat flux F_C [whether buoyancy-driven, $F_C \propto (T_c - T_a)^{4/3}$, or wind-forced, $F_C \propto T_c - T_a$] can be found by using parameterizations well established in other contexts (Wilson & Head 1883, Griffiths & Fink 1992a). For submarine eruptions the calculation is complicated by the large temperature differences, boiling (at lower pressures), and highly nonlinear properties of seawater at high temperatures and pressures (which lie near the critical point under water depths of >2 km) (Griffiths & Fink 1992b). Representative fluxes are plotted in Figure 3. Radiation dominates under the thin atmospheres of Earth and Mars, whereas the Earth's atmosphere has sufficient heat capacity that convection provides a comparable flux once the surface temperature has fallen to $< \sim 200^\circ\text{C}$. Radiation is less important than convection for temperatures of $< 900^\circ\text{C}$ under

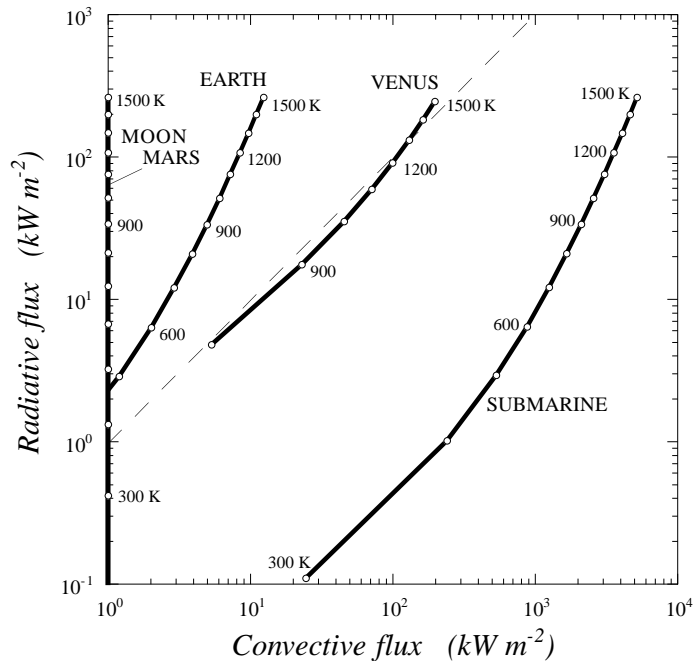


Figure 3 Estimated surface fluxes from lavas, owing to radiation (vertical axis) and free buoyancy-driven turbulent convection (horizontal axis), as functions of the lava surface temperature (in Kelvin). Recall that this temperature is much less than that of the interior. Fluxes from lavas on the Moon and Mars are shown along the vertical axis, because their atmospheres are too thin to give significant convective fluxes. The results for Venus are terminated at 800 K, because the lowland surface temperature is 750 K. Submarine fluxes are much larger than the others as a consequence of the large heat capacity of water. The oblique line represents $F_R = F_C$. (Adapted from Griffiths & Fink 1992a)

the dense atmosphere of Venus (where $T_a \approx 750^\circ\text{C}$). Underwater radiation is always negligible relative to the very rapid convective transport.

Surface cooling leads to solidification, which occurs through formation of an amorphous glass when quenching is rapid [cooling faster than $20\text{--}30^\circ\text{C s}^{-1}$ to the glass transition at 700°C (Leshner et al 1999, Keszthelyi & Denlinger 1996). If cooling is slower, solidification occurs by crystallization at temperatures below the solidus (around 1100°C). If crystallization is rapid (owing to either cooling or the exsolution of volatiles and the consequent increase in the liquidus temperature after eruption), the latent heat of crystallization may add significantly to the heat budget. As an example, crystallization in a Hawaiian channel flow traveling at $1\text{--}2\text{ m s}^{-1}$ was found to occur primarily by nucleation of new crystals, at the rate of $10^4\text{ crystals m}^{-3}\text{ s}^{-1}$ (or $0.2\text{--}0.5\text{ volume fraction h}^{-1}$) in response to a cooling rate of $22\text{--}50^\circ\text{C h}^{-1}$ (Cashman et al 1999b). This illustrates a rapid

cooling rate in the flow interior caused by stirring in a fast, highly disrupted flow and is in contrast to more viscous flows, in which the much slower cooling rates are controlled by conduction. However, quenching of the surface temperature for all flows is rapid, taking only 0.1 or 100 s to fall below the glass transition under water or air, respectively.

Cooling also occurs from the base of a flow by conduction into underlying rocks, leading to solidification at the bottom of the flow (if the flowing lava is cool enough or short lived) or to melting and erosion of the substrate (if the flow is sufficiently hot relative to the melting temperature of the base and advection continues long enough to supply sufficient heat; see Section 6.4). Melting is more readily accomplished by turbulent flows, because heat is drawn from throughout the flow depth. The latter scenario is relevant to komatiites (Huppert & Sparks 1985, Williams et al 1998), to lava tubes at channel bends and abrupt changes in slope (Kauahikaua et al 1998), and to basalt channels not far from the vent (Cashman et al 1999b).

5. FLOW REGIMES WITHOUT COOLING

5.1 Relevant Conditions

The first step in the formulation of useful dynamical models for lava flows is a consideration of the relevant dynamical regimes. Consider an eruption of lava from a localized vent at volume flux $Q(t)$, with viscosity η , yield stress σ_0 , and density ρ into an environment having ambient density ρ_a . The developing flow will have depth $h(x,y,t)$ and planform area $A(t)$. The eruption may be onto a horizontal plane, a sloping plane, or a more complicated topography such as a valley or mountain summit. Assuming the viscosity is constant (i.e. a Bingham fluid), the horizontal and vertical momentum equations can be written as

$$\rho Du_i/Dt = -\partial P/\partial x_i + (\partial/\partial y + \partial/\partial z)[2(\eta + \sigma_0/\dot{\epsilon})(\epsilon_{ij} - 1/3\nabla \cdot \mathbf{u}\delta_{ij})] \quad (5a)$$

$$\begin{aligned} \rho Dw/Dt = \rho g - \partial P/\partial z + (\partial/\partial x + \partial/\partial y) \\ [2(\eta + \sigma_0/\dot{\epsilon})(\epsilon_{ij} - 1/3 \nabla \cdot \mathbf{u}\delta_{ij})], \end{aligned} \quad (5b)$$

where u_i and w are horizontal and vertical components of velocity, $D\mathbf{u}/Dt = \mathbf{u}_t + \mathbf{u} \cdot \nabla \mathbf{u}$, and $g = g^*(\rho - \rho_a)/\rho$ is the reduced gravity (the gravitational acceleration g^* is in the negative z direction), P is pressure, $\epsilon_{ij} = 1/2[(\partial u_i/\partial x_j) + (\partial u_j/\partial x_i)]$ are components of the rate of strain tensor, $\dot{\epsilon}$ is again the magnitude of the shear rate, and δ_{ij} is the delta function. For flow on a plane of slope β from the horizontal, it will normally be convenient to recast these equations into coordinates parallel and normal to the slope, which changes the gravitational term in Equation 5b to $\rho g \cos \beta$ and introduces a term $\rho g \sin \beta$ into Equation 5a.

In a suitably nondimensionalized form and dropping for convenience the final term representing the strain associated with compressibility (although this may be significant in flows with large bubble contents), Equation 5a becomes

$$ReDu_i/Dt = G (H/L)\partial P/\partial x_i + (H/L\partial/\partial y + \partial/\partial z)[2(1 + B)\varepsilon_{ij}], \quad (6)$$

where velocities have been scaled by U , vertical lengths by H , horizontal lengths by L , time by H/U , and pressure by ρgH . The dimensionless parameters are the Reynolds number $Re = \rho UH/\eta$, the ratio of buoyancy to viscous stresses $G = \rho gH^2/\eta U$, the aspect ratio H/L of the flow, and the Bingham number $B = \sigma_0/\eta\dot{\varepsilon} = \sigma_0 H/\eta U$. For $Re \ll 1 + B$, the inertia effects are negligible, and the internal stresses are balanced by the gravitationally induced stress ($G \approx 1$). The aspect ratios of lava flows range from $H/L \approx 0.2$ – 0.3 for most lava domes (based on their radius) and ~ 0.1 for pahoehoe toes to very small values (< 0.01) for long-channel and sheet flows.

The Reynolds number can be evaluated from estimated speeds, depths, and viscosities of flows observed while they were active. For the slow effusion of very viscous lavas forming domes, which on Earth are tens of meters high and 10^2 – 10^3 m across, $Re \sim 10^{-10}$ – 10^{-4} . Hence modeling of these flows has started with solutions for the spreading of very viscous Newtonian fluid creeping over horizontal or sloping planes (see Section 5). The relatively rapid channel flows on Hawaii, on the other hand, have velocities on the order of 10 ms^{-1} near the vent and 0.1 ms^{-1} near the flow front, depths of 1–10 m, and viscosities near the vent on the order of 10^3 Pas, hence $Re \sim 1$ – 10^2 , becoming smaller downstream as the viscosity increases and slope decreases (Cashman et al 1998, 1999b). Ancient eruptions of very hot komatiite lavas are thought to have had velocities on the order of 10 ms^{-1} , viscosities of ~ 1 Pa, and depths of ~ 10 meters, which suggest values of Re possibly as large as 10^6 (Huppert & Sparks 1985, Huppert et al 1984). Hence these ancient flows would have been turbulent with efficient mixing throughout the depth of a flow, whereas the largest of present-day flows, although not fully turbulent, are strongly agitated by irregularities in the channel and by blocks of solid lava carried by the flow. Thus the modeling of long basalt flows (see Section 6.3) has started from the assumption of well-mixed channel flows having properties that are uniform in the vertical. An additional consideration for flows with large Re is that surface gravity waves can propagate without immediate dissipation. Hence the Froude number $Fr = U/\sqrt{gH}$ [$= (Re/G)^{1/2}$ in 6] is a relevant parameter, and, if $Fr > 1$, the lava flow potentially involves control points, supercritical flow, and hydraulic jumps.

Evidence for non-Newtonian flow regimes is obvious on many lava flows, including linear crevasse structures, along which the material parts as it is slowly extruded (termed creases; Anderson & Fink 1986), irregular surfaces sometimes dominated by tall angular spines, smooth striated extrusion surfaces, tearing of the surface lava in channel flows, and the formation of solidified levees that channelize Hawaiian lavas. In the Bingham fluid approximation, the significance

or otherwise of a yield stress is determined by the value of the Bingham number B in Equation 5. For Newtonian flow, $B = 0$, whereas $B \rightarrow \infty$ for those parts of a flow having very small shear rate $\dot{\epsilon} \ll \sigma_0/\eta$ or a large yield stress $\sigma_0 \gg \dot{\epsilon}\eta$. For small Re , $B \ll 1$ implies a viscous-gravity balance, whereas $B \gg 1$ implies a balance of yield stress and gravity in which the flow depth scales as $H \sim (\sigma_0 L/\rho g)^{1/2}$.

Lava flows lie across the full range of B . For example, the dome of basaltic andesite that was erupted on La Soufrière volcano on the island of St. Vincent in 1979 (Huppert et al 1982), had a height of 100 m, a front velocity of $3 \times 10^{-5} \text{ ms}^{-1}$ (400 m in 150 days), and an interior apparent viscosity $\eta_A \sim 2 \times 10^7 \text{ Pas}$ (a petrologic prediction given the observed 45% crystallinity and eruption temperature of 1000°C). If the yield stress is on the order of $\sigma_0 \sim 10^5 \text{ Pa}$ (consistent with values obtained in the laboratory for similar lava samples, Murase & McBirney 1973), we estimate $B \sim 10^4$. There are of course uncertainties of an order of magnitude in both the viscosity and yield stress used here. Nevertheless, it is clear that $B \gg 1$ for this dome. Measurements available for a number of other lava domes lead to a similar conclusion—that silicic domes tend to grow so slowly that the viscous stresses are very small compared with the yield stress, and therefore the domes are effectively, at any moment, in a static equilibrium between gravity and yield stress (Blake 1990). When the effects of cooling are taken into account, a carapace yield stress may be much greater than the interior strength used above, and it has been argued (Griffiths & Fink 1993, 1997; see Section 6.2) that this further increases the effective value of B by several orders of magnitude.

At the other end of both the flow rate and rheologic spectrum, large basaltic channel flows have strain rates $U/H \sim 0.1\text{--}1 \text{ s}^{-1}$, viscosity of $\sim 10^3 \text{ Pas}$, and a small or vanishing yield stress. Hence $B \ll 1$, as long as $\sigma_0 \ll 10^3 \text{ Pa}$, and the flow can be considered to be viscous. This is the case near the vent and, for Hawaiian flows, a kilometer or two down-channel. However, the crystallinity will eventually reach the critical value of 45%–50% as a result of cooling and stirring (observed, e.g. Cashman et al 1999b). This can be hastened by the exsolution of volatiles. Hence the onset of a yield stress $>10^3 \text{ Pa}$ can be expected, and there may be a transition in flow regime. The viscous stresses may remain important in regions of greatest shear, but plastic deformation at $\dot{\epsilon} < \sigma_0/\eta$ will dominate in cooler and slower parts of the channel. Note that Hulme (1974) estimated transitional flow strengths of $10^2\text{--}10^4 \text{ Pa}$ on many basaltic channel flows using the height of levees, ground slope, and lava density in an isothermal model (see Section 4). A similar conclusion applies to smaller breakouts from these channels, forming relatively shallow pahoehoe flows characterized by a thin glassy skin. In these the shearing rate is closer to 0.1 s^{-1} , and the critical yield stress (that giving $B = 1$) for the interior is $\sim 10^2 \text{ Pa}$. Again, however, cooling of the surface may dominate, and in this case it is unclear whether the glass is best treated as a much more viscous layer or as a thin, strong boundary layer containing the underlying low-viscosity fluid. The results of Bingham flow models applied to lava flows

have been fruitful in accounting for various aspects of real flow behavior and are discussed in Sections 5.4 and 5.5 (isothermal models) and 6 (effects of cooling).

5.2 Axisymmetric Viscous Flow

Under the assumptions of small Re , constant viscosity, hydrostatic pressure, $H/L \ll 1$, and axisymmetric motion on a horizontal plane, Equations 5a and b reduce to

$$\partial P/\partial r = \rho g \partial h/\partial r = \eta \partial^2 u/\partial z^2, \quad (7)$$

where $u(r,z,t)$ is the radial velocity. The problem is closed by continuity and the conditions of zero velocity at the base $z = 0$ and zero stress at the top of the flow $z = h$. It is straightforward to find the dependence of flow radius R and depth H on time implied by Equation 7 by comparing the integrated gravitational driving force $F_B \sim \rho g H^2 R$ to the retarding force $F_\eta \sim \varepsilon \eta R^2$ caused by shear stress acting over the basal area (Lister & Kerr 1989, Blake 1990, Griffiths & Fink 1993). Under the self-similarity assumption, continuity implies $V \sim HR^2$. For dome volumes varying with time as $V = St^\alpha$, where S and α are constants ($\alpha \geq 0$) (Huppert 1982b),

$$R \sim [\rho g S^3/\eta t^{(3\alpha+1)}]^{1/8}, \quad H \sim [\eta S/\rho g t^{(\alpha-1)}]^{1/4}. \quad (8a)$$

These expressions also give the speed u_f of flow front advance and a relation between height and radius

$$u_f \sim [\rho g S^3/\eta t^{(3\alpha-7)}]^{1/8}, \quad H \sim [(\eta/\rho g)^\alpha S R^{(2\alpha-2)}]^{1/(3\alpha+1)}. \quad (8b)$$

A complete similarity solution that provides values for the constants of proportionality omitted in Equation 8, as well as the flow shape $h(r)$, was given by Huppert (1982b) and Huppert et al (1982). The solution agrees well with laboratory experiments using viscous oil spreading on a plane. Interesting conclusions from Equation 8a are that the radius of a flow of constant volume ($\alpha = 0$) increases as $t^{1/8}$, so that the rate of advance of the front becomes extremely slow after a short time, while the height decreases. For a constant source flux ($\alpha = 1$), the radius increases as $t^{1/2}$, velocity decreases as $t^{-1/2}$, and the height is constant at $(\eta S/\rho g)^{1/4}$. Dome height increases with time only if the source flux (or viscosity) increases with time. Flow from the vent in such a viscous model is largely accommodated by divergent radial motion near the flow surface, and the flow front advances through upper levels of the fluid moving to the flow front, where they are subsequently overrun.

In an application of the results to the Soufrière dome by Huppert et al (1982), the dome volume during the first 90 days of dome growth was fitted by the power-law expression $V \sim t^{1.36}$ (i.e. $\alpha = 1.36$). Based on this fit the predicted behavior of the radius is $R \sim t^{0.63}$, whereas the measurements give $R \sim t^{0.58}$. If this is taken as a reasonable agreement, a rearrangement of Equation 8a into the form $\eta \sim \rho g S^3 t^{(3\alpha+1)}/R^8$ can be used to estimate the viscosity, giving $\eta \sim 2 \times 10^{11}$ Pas.

However, this approach is problematic. The viscosity obtained is inaccurate because it is proportional to high powers of the measured volumes and radii. The mean value obtained is also ~ 4 orders of magnitude greater than that given by petrologic methods. In addition, the dome height increased more rapidly than the model predicts. These discrepancies were attributed to non-Newtonian properties, the effect of a cooled skin or the effects of a flow front composed of cooled lava and avalanched blocks. On the other hand, this implies that application of the uniform viscosity solution does not capture the essence of the controls on the spread of the lava. We will also see below that the similarity between the predicted and measured power-law exponents for the dome radius does not discriminate well between differing mechanisms of deformation.

5.3 Viscous Flow On A Slope

The spreading of a Newtonian fluid on a sloping plane can be described under the same approximations as in Section 5.2, but this time the flow is not axisymmetric, and it becomes necessary to solve for the flow outline as well as the three-dimensional depth distribution. Analyses of the shape of an evolving flow from point and line sources on a plane of slope angle θ are given by Lister (1992) and tested by laboratory experiments using various viscous fluids. The similarity solutions for a point source show that the flow becomes strongly influenced by the slope at a time T^* or a volume $V^* \sim ST^{*\alpha} \sim S[(\rho g/3\eta S)^{-1} \cot^5\theta/\sin\theta]^{1/(\alpha+3)}$, where the notation is that used in Equation 8. At larger times the across-slope flow width W increases as $W \sim (S\cot\theta t^\alpha)^{1/3}$, whereas the down-slope length increases as $L \sim (\rho g/3\eta)^{1/3} [S^4 t^{4\alpha+3} \sin^5\theta/\cos^2\theta]^{1/9}$. The corresponding flow depth near the vent varies as $H \sim (\rho g/3\eta)^{-1/3} [S^2 t^{2\alpha-3}/(\cos\theta \sin^2\theta)]^{1/9}$. The ratio of across-slope width to down-slope length varies with time as $W/L \sim t^{(\alpha+3)/9}$ and can be expressed in terms of the total volume released onto the slope:

$$W/L \sim (\rho g/3\eta S^{1/\alpha})^{1/3} (\sin^8\theta/\cos^5\theta)^{1/9} V^{(\alpha+3)/9\alpha}. \quad (9)$$

Thus, for the particular case of a constant source flux ($\alpha = 1$), we have $L \sim t^{7/9}$, $W \sim t^{1/3}$, and $H \sim t^{-1/9}$. In this case we also have $W \sim L^{3/7}$ and W/L proportional to $\eta^{-1/3}$, $Q^{-1/3}$, and $V^{4/9}$. For larger viscosity and larger volume flux, the flow is more elongated, whereas it grows wider (compared with its length) as the volume increases. These results provide a useful basis for comparison when assessing the results of theories or experiments with different fluid rheology or the effects of cooling, and they may help to understand the shape of, for example, large rhyolite flows on slopes (Figure 1e).

Surface tension was found to have significant effects at large times in the experiments of Lister (1992), leading to a surface tension-dominated rivulet at the down-slope extremity of the flow or to bifurcation in a fingering-style instability (Huppert 1982a). However, surface tension is negligible on scales greater than a few centimeters in real lava flows, and it will not influence flow spreading

for all but perhaps small pahoehoe “toes.” Flow branching is instead caused by rheology variations from cooling (see Section 6).

5.4 Axisymmetric Viscoplastic Flow

The introduction of a yield strength into the simplest flow problem above—the slow axisymmetric spreading of a thin layer of fluid from a small vent—is highly instructive. Blake (1990) proposed that the material of highly silicic lava domes possesses a yield strength and replaced Equation 7 with the static balance obtained from Equation 5 for $B \gg 1$:

$$\partial P/\partial r = \rho g \partial h/\partial r = \sigma_0/h. \quad (10)$$

This model is based on the assumption that the fluid does not deform anywhere but at its base, where the pressure is greatest and, for the fluid to have reached its current shape, equal to the yield stress. The solution to Equation 10, originally given by Nye (1952) in the context of icesheet dynamics, with $h = 0$ at $r = R$, is simply

$$h^2 = (2\sigma_0/\rho g)(R - r), \quad (11)$$

which implies that the central height $H = h(0)$ and the radius R are always related by $H = C(\sigma_0 R/\rho g)^{1/2}$, where $C = \sqrt{2}$. Using slurries of kaolin powder in water, Blake (1990) found excellent agreement for the shape, except at the origin—where transition from vertical flow in the small vent to lateral flow outside necessarily involves strain rates large enough for viscous stresses to become significant and the surface slope discontinuity disappears—and at the flow front where the flow is steeper than the solution.

Scaling analysis starting from the integrated force balance $g\rho H^2 R \sim \sigma_0 R^2$ and the self-similar continuity relation $V \sim HR^2$, and again assuming dome volume varies as $V = St^\alpha$, leads to

$$\begin{aligned} R &\approx 0.65(\sigma_0/\rho g)^{-1/5} S^{2/5} t^{2\alpha/5}, \quad H \approx 1.4(\sigma_0/\rho g)^{2/5} S^{1/5} t^{\alpha/5}, \\ H &\approx 1.76(\sigma_0 R/\rho g)^{1/2}, \end{aligned} \quad (12)$$

where the constants shown are the empirical values (obtained for constant volume flux), and we note that, in $H(R)$, the value $C \approx 1.76$ is somewhat larger than predicted. These scaling laws are also consistent with results obtained from isothermal experiments with slurries of kaolin in polyethylene glycol wax spreading under water (recall that g is the reduced gravity; Griffiths & Fink 1997), but in that case σ_0 and C were not evaluated independently. The most interesting aspect of this solution is that the relation between H and R is independent of time and also independent of S and α —the solution is a static one. Thus, when the vent flow is stopped in the experiments, the dome does not continue to flow as it does in the viscous case. Also in contrast to the viscous flows, marked elements of the flow surface moved radially but did not approach the flow front, and the same

material remained at the front throughout the spreading. There are two sets of slip planes spiraling out from the summit, which divide the surface into small roughness elements. The surface roughness remained small under air as a result of surface tension but was several millimeters high under water for the slurries used.

Since shear rates are larger near the vent, viscous stresses can be more important when R/H is small. Hence there can be a transition from viscous flow ($B \ll 1$) at small times to plastic flow ($B \gg 1$) at large times (Blake 1990). From the results for Newtonian flow (8), we see that $B \ll 1$ for $t \ll [(g^3 \rho^3 \eta^5 S) / \sigma_0^8]^{1/5(5-\alpha)}$ and that transition to plastic flow will always occur for $\alpha < 5$.

Application of this uniform-yield stress model to the Soufrière lava dome is straightforward, because the volume and time are not needed; the measurements give $H \sim R^{0.52}$, in very good agreement with Equation 12. Using the power-law relation for $V(t)$ as fitted to the measurements by Huppert et al (1982), Equation 12 also predicts $R \sim t^{0.544}$ and $H \sim t^{0.272}$, both of which are closer to the observed trends than are those predicted by the Newtonian model. Given this agreement, evaluation of the yield stress from $H/R^{1/2}$ by using Equation 12 gives $\sigma_0 = 2.6 \times 10^5$ Pa for Soufrière and similar values for a number of other domes. Thus the plastic model appears to describe lava domes better than does the viscous model.

The axisymmetric solutions for viscous and plastic flows have been extended to viscoplastic (Bingham) flow at $B < 1$, conditions in which both viscous stresses and yield stress are significant (Balmforth et al 1999). These authors also investigated the effects of shear thinning of a power-law fluid by using the Herschel-Bulkley rheology (Equation 3), and they concluded, from numerical solutions for constant volume flux, that it may be difficult to differentiate between the effects of yield stress and shear thinning. However, as we have seen above, the Bingham numbers for lava domes (based on crude estimates for the yield stress and viscosity) are so large that viscous stresses, whether linear or dependent on a higher power of the shear rate, are expected to be negligible. Note also that the isothermal experiments by Griffiths & Fink (1997; carried out as isothermal comparisons to cooling flows) gave final static shapes that did not alter when the source flux was turned off and that recent experiments on a slope (Osmond & Griffiths 1998; discussed in Section 5.4) involved constructing a large dome with a series of small incremental extrusions separated by long repose periods and yet gave identical dome shapes (at the same volumes) to runs with continuous extrusion. Thus the dome shape appears independent of volume flux history and shear rate so long as extrusion rates are small. As quantified above, lava domes too have very small extrusion rates, and some (e.g. the Mt. St. Helens dome, which grew from 1981 to 1986) are similarly constructed by many sequential extrusions.

An interesting aspect of radially expanding Bingham flows is that the pressure gradient is assumed to be too small everywhere to cause deformation except at the base, where the yield stress is attained. Hence a plug flow is predicted. How-

ever, the motion described by the continuity equation, integrated over the depth to give

$$\partial h/\partial t + 1/r \partial/\partial r(rU) = w_s, \quad (13)$$

where $U(r,t) = \int_0^h u(r,z,t) dz$ and w_s is the vertical velocity at the free surface, is actually extensional in the azimuthal direction and compressional in the radial direction (Blake 1990). Hence there is no true plug flow, and the fluid is deforming everywhere. Balmforth & Craster (1999) and Balmforth et al (1999) addressed this paradox and showed, through an expansion in the aspect ratio $H/L \ll 1$, that the plug flow is valid only at leading order. The fluid is actually weakly yielding throughout its depth, to compensate for the radial expansion, and $\partial u/\partial z \sim O(H/L)$.

Another axisymmetric non-Newtonian model, one that incorporates a heterogeneous rheology resulting from heat loss, consists of a uniform (viscous) interior capped by a thin brittle shell having a tensile strength (Iverson 1990). In this case, the static balance between gravity and tensile strength in the shell gives an elliptic height profile that is wider and lower for smaller tensile strengths. The model does not include the thermodynamics, which control the crust thickness, but the dome is proposed to grow with added volume input through brittle failure of the crust followed by quenching to form a crust in equilibrium with the new volume.

5.5 Viscoplastic Flow on a Slope

Early realization that the levee banks created by long basalt flows implied non-Newtonian flow led Hulme (1974) to consider the unconfined motion of a Bingham fluid down a plane of slope β . He considered long flows and assumed that all quantities are independent of the distance x down-slope. Near the edges of the flow its depth $h(y)$ becomes small, and the lateral flow is assumed to cease when the cross-slope pressure gradient is balanced by the basal-yield stress, as expressed in Equation 10 (with the radial coordinate r replaced by the cross-slope distance y). The cross-slope depth profile near the edges is then fixed and given by Equation 11 (with the radius R replaced by the cross-slope width W of the whole flow). This balance also gives the depth $H = C(\sigma_0 W/\rho g)^{1/2}$ on the center line of the flow. If the flow depth is assumed to be constant in the down-slope direction at any value of y , then motion requires $\rho g h(y) \sin \beta > \sigma_0$. Hence there is a critical depth

$$h_s = \sigma_0/\rho g \sin \beta, \quad (14)$$

below which there will be no down-slope motion. Substituting this depth into the cross-slope balance (Equation 10) gives the width of the region of stationary fluid along the edge of the flow:

$$w_s = \sigma_0/2\rho g \sin^2 \beta = h_s/2 \sin \beta. \quad (15)$$

Between these two stationary regions, there is free viscoplastic flow down-slope, which Hulme approximated as the two-dimensional flow between a parallel stress-free surface and the bottom plane, leading to the depth-averaged velocity (Skeland 1967, Hulme 1974):

$$u = (\rho g \sin \beta h_s^2 / 3\eta) [(h/h_s)^3 - 3/2(h/h_s)^2 + 1/2]. \quad (16)$$

A problem with the analysis is that, for the cross-slope motion to cease, it is necessary to consider more than the cross-slope component of the basal stress; the total stress $\sigma = \rho gh[\sin^2 \beta + (\partial h/\partial y)^2]^{1/2}$ at the base (where the down-slope thickness gradient is neglected) must become equal to the yield stress.

Hulme's (1974) laboratory experiments with kaolin-water slurry on a slope revealed the presence of stationary levees bounding long down-slope flows. The height of the levees was consistent with the formula, which was then applied to lava flows to find yield strengths (of $\sim 10^3$ Pa for low silica contents to 10^5 Pa for higher silica contents) for various flows given the height of levees (5–30 m) and the underlying topographic slope. This much of the behavior of long flows, and particularly the observed levees, can therefore be explained in terms of isothermal flows having a yield strength. The levee-derived correlation between silica content and strength for terrestrial flows, along with remote measurements of levee heights, was even used to estimate compositions of lunar flows. In detail the real flow levees are formed of cooled flow-front or surface material (discussed in Section 6) pushed aside by the advancing flow front, so that only the levees are required to have a yield strength. However, the principle and the application of Equation 14 are unchanged.

A more difficult problem is posed by large lava domes on slopes; these are not the very long flows described by Hulme (1974). Instead, the challenge is to predict the fully three-dimensional shapes, including the extent of up-slope flow from the vent. A solution can be found for the three-dimensional case in the limit of slow flows ($B \rightarrow \infty$) and gives the final width of very long down-slope flows independent of the viscosity. We again assume $H/L \ll 1$, a hydrostatic gradient in the vertical, and a static balance between gravity and yield stress (this time in the plane parallel to the base slope), and we obtain an equation for flow thickness $h(x,y)$ normal to the base (Osmond & Griffiths 1998):

$$(\partial h/\partial x - \tan \beta)^2 + (\partial h/\partial y)^2 = (\sigma_0/\rho gh \cos \alpha)^2. \quad (17a)$$

Assuming symmetry about the down-slope (x) axis through the source implies $\partial h/\partial y(y=0) = 0$ (except at $x=0$, where $\partial h/\partial y$ must be discontinuous to force radial flow from the vent). Then Equation 17a can be solved for the thickness profile $h(x,0)$. Scaling thickness h by h_s (Equation 14) and distance x parallel to the slope by $h_s/\sin \beta$ leads to the dimensionless thickness profiles

$$\begin{aligned}
 x &= h - H + \ln |(1 - h)/(1 - H)|, \quad x \geq 0 \\
 &= h - H - \ln |(1 + h)/(1 + H)|, \quad x \leq 0, \quad (17b)
 \end{aligned}$$

on the down-slope ($x > 0$) and up-slope ($x < 0$) sides, where $h = H$ at $x = 0$. The leading edges of the flow are found at $h = 0$, and from Equation 17b we have

$$x_d = -H - \ln |1 - H|, \quad x_u = -H + \ln |1 + H|, \quad (17c)$$

or a total flow length $L = -\ln |1 - H^2|$. The cross-slope thickness profile of the dome can be approximated by neglecting $\partial h/\partial x$ in Equation 17a in the region of maximum width (down-slope from $x = 0$), and the maximum width is given by $W \approx 2[1 - \sqrt{1 - H^2}]$. It tends to be more useful to describe these flows in terms of their volume V at any time, where V is normalized by the volume scale $\sigma^3/(\rho g)^3(\sin^5\beta)$; the dome is not much influenced by the topography for $V \ll 1$ but strongly influenced and displaced somewhat down-slope from the vent for $V > 1$.

When $V \gg 1$ (and the thickness H tends to 1), the down-slope length of the dome tends to infinity. This reflects the fact that Hulme's (1974) critical thickness h_s (Equation 14) is the maximum dome thickness that can be supported on the slope in a static balance. For $V \ll 1$ (i.e. $H \ll 1$ as a result of small volume, large yield strength, small slope, or reduced gravity), the dome is not influenced by the base slope and is close to axisymmetric, and the solution (Equation 17b) approaches the quadratic profile (Equation 11). To obtain the dome perimeter and contour plots of flow thickness as a function of H (or of total flow volume V) Equation 17a was solved numerically. [A very similar problem is treated through numerical simulation by Miyamoto & Sasaki (1998).] The solutions can be compared with isothermal experiments with slurries of kaolin in polyethylene glycol wax as well as kaolin in water, both on a sloping base (Figure 4). For $V \approx 0.1$ ($H \approx 0.7$), the flow margin begins to depart noticeably from circular, and the down-slope length is more than twice the up-slope length from $x = 0$. For $V \approx 1.5$ ($H \approx 0.95$), the down-slope length is eightfold greater than the up-slope length and nearly twice the full width. The stationary levees of Hulme (1974) are seen to form along the edges of the down-slope flow at very large flow elongations ($V > 10$, $H \rightarrow 1$; Figure 4b). The laboratory flows tended to spread farther across slope and were less elongated than predicted, but are otherwise consistent with the theoretical solution. Two sets of slip planes again curve out from the summit as in Blake's (1990) experiments on a horizontal base, but this time they are asymmetric in the x direction. In the analysis the assumption of the static balance everywhere implies that the origin is to be identified with the vent from which the fluid was supplied. There is no implication that fluid volumes having histories different from this will take similar shapes; the static shape will be different if the base slope is changed after the volume is emplaced or if the flow is viscous for a time before taking on a yield strength.

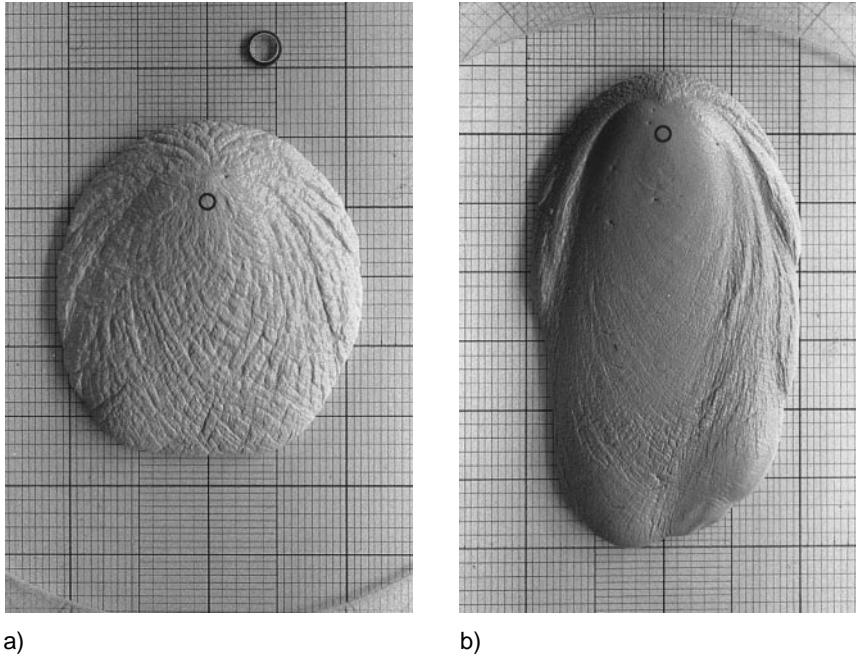


Figure 4 Photographs of isothermal laboratory flows of Bingham fluid on a planar slope. The fluid was extruded in many small-volume increments from a 1-cm-diameter hole in the smooth base. The domes were static between increments. The *white circle* shows the location of the source. (a) Kaolin/water slurry, slope $\beta = 12^\circ$, volume 900 cm^3 , $\sigma_0 = 92 \text{ Pa}$, dimensionless volume $V \approx 0.8$ (b) Kaolin/polyethylene glycol slurry, $\beta = 18^\circ$, 1000 cm^3 , $\sigma_0 = 84 \text{ Pa}$, $V \approx 12$. ‘Levees’ develop for $V > 10$, when further spreading is largely down-slope. (From Osmond & Griffiths 1998)

6. EFFECTS OF COOLING AND SOLIDIFICATION

6.1 Dimensionless Parameters

Since lavas are far from thermal equilibrium with the overlying atmosphere or ocean and relatively close to their solidus temperatures, cooling induces very large changes in rheology that eventually bring flows to a halt. It is therefore important to investigate thermal effects in flow models. These effects depend on whether the flow is laminar or turbulent and on the rate of cooling and rheological change compared with the rate of spreading of the flow. Comparing the conductive transport of heat within the lava to the advection of heat with the flow gives Peclet (Pe) numbers $Pe = UH/\kappa$ (κ is the diffusivity) ranging from 10^2 to 10^5 for slow-growing lava domes to $>10^6$ for faster channelized basalts and turbulent komatiite flows. As a measure of the rate of cooling, we could take the global Nusselt (Nu) number, $Nu = F_s^*H/\rho c_p \kappa \Delta T$, based on the surface heat flux F_s^* that would occur

if the contact temperature remained at the eruption temperature T_e . This Nu number can be rewritten as $Nu \sim H/\delta_T$, where δ_T is the thickness of a steady-state conductive layer that can supply the surface flux F_s^* . (Alternatively, the ratio $Nu_A = F_s^*/(\rho c_p \Delta T U) = Nu/Pe$ based on the advective heat transport might be used.) Taking as an example an eruption temperature $T_e \approx 1150^\circ\text{C}$, $T_a \approx 0^\circ\text{C}$ and the fluxes from Figure 3, we find $Nu \sim 10^3$ (for all subaerial flows) (and $Nu_A \sim 1$ or 10^{-3} for domes and fast-flowing basalts, respectively). The large values of Pe and Nu indicate that active flows, whether they are laminar or turbulent, will involve only thin thermal boundary layers. The small values of Nu_A indicate that the surface fluxes are sufficiently small that lavas can flow a large distance (if the velocity U is sustained) before being completely cooled. For laminar flows (while they remain shorter than $L \sim H Pe^{1/2}$), the interior is not cooled, and the flow must become thermally and rheologically stratified. For turbulent flows, mixing of the surface boundary layer into the interior may be possible (if mixing is not inhibited by rheological contrasts) and will cool the interior with distance downstream. When the flow involves crystallization (or melting of the floor), the latent heat of fusion L_h can be significant compared with the specific heat, as measured by the Stefan number $S = L_h/c_p \Delta T$, and should be included in any complete heat budget. However, it is generally a small effect.

Note that cooling has its influence through variations in the lava rheology, whereas the Pe and Nu numbers concern only the temperature distribution. The strong dependence of rheology on temperature near the solidification temperature introduces a complexity but increases the validity of the simplifying thin-boundary-layer-and-isothermal-interior approximation for both laminar and well-mixed flows. Because the most dramatic rheological changes with temperature are caused by solidification, they occur at temperatures close to the glass transition temperature (under rapid cooling) or at temperatures for which the crystallinity passes through the critical range 40%–60% (for slow cooling). We are concerned with rapid surface quenching and a glassy crust on all flows. For turbulent flows there are, in addition, the effects of mixing and relatively slow distributed cooling, hence crystallization and consequent change of rheology, in the bulk of the flow. An important parameter that determines the extent of solidification is $\Theta_s = (T_s - T_a)/(T_e - T_a)$, the proximity of the eruption temperature T_e to the solidification temperature T_s . For $\Theta_s \ll 1$, a large amount of cooling is required to reach solidification, whereas, for $\Theta_s \approx 1$, there is rheological change with little cooling. Basaltic lavas (with $T_e \approx 1150^\circ\text{C}$, $T_a \approx 0^\circ\text{C}$, and a glass transition at $T_s \approx 700^\circ\text{C}$) have $\Theta_s \approx 0.6$, and highly silicic lavas (with $T_e \approx 900^\circ\text{C}$) have $\Theta_s \approx 0.8$.

Although the set of thermal parameters (Θ_s , Nu, and Pe) (or Θ_s and a flux-modified Pe number; Fink & Griffiths 1990) are sufficient to define a cooling and solidifying flow at small Re and given rheology, it is possible to define a dimensionless parameter that provides a more ready indication of the extent and effects of solidification. In the thin boundary layer regime, surface solidification commences at a distance $d_s \approx ut_s$ from the vent, where u is the surface velocity and t_s is the time taken for the surface temperature T_c to cool from the vent temperature

T_e to the solidification temperature T_s . Scaling distance by H and velocity by a suitable scale U , we define the dimensionless parameter

$$\Psi = Ut_s/H = t_s/t_A \quad (18)$$

or, equivalently, $d_s/H \approx \Psi$, where $t_A = H/U$ is the time scale for lateral flow through a distance H (Fink & Griffiths 1990, Griffiths & Fink 1993). The value of t_s depends on Θ , and the surface heat flux, and it must be obtained from a heat transfer calculation, accounting for radiation and convection from the surface (Griffiths & Fink 1992a,b). This solidification time is on the order of 0.1 s for submarine lavas, 100 s for subaerial basaltic lavas (on Earth and Mars), and ~ 60 s for the cooler highly silicic lavas under air. The parameter Ψ is defined for extrusions of constant volume flux Q in terms of the advective time scale t_A appropriate to the corresponding isothermal Newtonian gravity currents of Section 5.2. A similar parameter Ψ_B can be defined, again by Equation 18, when the flow is plastic (Griffiths & Fink 1997). For the Newtonian case (and point source), a global velocity scale $U \sim Q/H^2 \sim (\rho g Q/\eta)^{1/2}$ and depth scale $H \sim (Q\eta/\rho g)^{1/4}$ (from Equation 8) give $t_A = (\eta/\rho g)^{3/4} Q^{-1/4}$. The dimensionless solidification time becomes

$$\Psi = (\rho g/\eta)^{3/4} Q^{1/4} t_s. \quad (19a)$$

For the plastic case, $U \sim Q(\rho g/\sigma_0)^2$ and $H \sim \sigma_0/\rho g$ lead to

$$\Psi_B = (\rho g/\sigma_0)^3 Q t_s. \quad (19b)$$

These definitions represent an attempt at describing a flow in a global sense, recognizing that the advection velocity at a given radius can vary with time (as the depth changes or the flow becomes nonaxisymmetric) and depends on distance from the vent. Thus there remains scope for time dependence of the effects of solidification within a flow having a fixed value of Ψ . Of course, variations of source volume flux lead to changes in Ψ .

At distances from the vent greater than d_s , the layer of solid crust will thicken in a manner that, again, can be calculated by coupling conduction in the lava to the surface heat flux through the surface temperature $T_c(t)$ (Griffiths & Fink 1992a,b). Note that, in terms of the external dimensionless parameters, Ψ and Ψ_B provide a general indication of whether the crust thickens quickly or slowly relative to the lateral motion, and they are more relevant to the thickness of the rheological boundary layer than is Pe , at least at early times, because the latter relates only to the thickness of the thermal boundary layer (given by $\delta_T \sim (\Psi/Pe^{1/2})H$ at the location of the onset of solidification).

Finally, the effects of cooling on flow dynamics depend on the magnitude of the rheological changes. A surface layer is most simply characterized by a constant crust viscosity η_c and yield strength σ_c . These (taken with crust thickness) suffice to parameterize a more continuous variation with depth, but are crude approximations when the properties may vary with time or location on the surface. On the other hand, they lead to a better representation of the dynamics than does

the use of a single apparent (bulk) flow viscosity η_f that increases with time as the flow enlarges (Huppert et al 1982, Stasiuk et al 1993). It can also be argued that the surface temperature of creeping flows is everywhere far below the solidification temperature so that the crust properties (but not crust thickness) will be roughly constant. The contrasts with the flow interior (η_c/η and σ_c/σ_0), along with crust thickness, will determine whether the crust remains passive or inhibits motion of the underlying fluid.

6.2 Creeping Flows with Cooling

Laboratory analog experiments serve to test the hypothesis that the primary effects of cooling and solidification for slow laminar flows are captured by Ψ , which can be seen as the ratio of the rate of lateral advection of fluid to the rate of solidification. The experiments used viscous polyethylene glycol (PEG) wax, which freezes at a convenient temperature of 18–19°C, extruded from a small (or linear) vent under cold water onto a horizontal or sloping base (Fink & Griffiths 1990, Fink & Griffiths 1992). The cold water gave a suitable turbulent convective heat flux and solidification times comparable to horizontal advection times. The results revealed a sequence of flow regimes (Figure 5), and these correlated with intervals of Ψ . At $\Psi < 0.7$, where cooling is rapid or extrusion is slow, the flow was fully encased in solid and spread through many small bulbous outgrowths reminiscent of submarine lava “pillows”; at $0.7 < \Psi < 2.5$, thick solid extended over most of the surface and formed rigid plates separated by divergent rifts, complete with transform faults, where solid continued to accrete onto the plates; at $2.5 < \Psi < 6$, solid became more widely distributed (except over the vent) but was thin and tended to buckle or fold, forming many small transverse ridges and ropy structures; at $6 < \Psi < 16$, crust was seen only around the margins of the flows, where it formed levees; and at $\Psi > 16$, no solid crust formed before the flow front reached the side walls of the container (the values of Ψ given here are smaller, by a factor of $10^{2/3}$, than those originally reported because an incorrect value for the water viscosity was originally used). In addition, the flows ceased to spread when the source flux was turned off if $\Psi < 6$, indicating control by the strength of the solid. The forms of surface deformation and flow morphology observed are similar to some of the main characteristics found on basaltic (low-viscosity) lava flows and traditionally used to categorize them. In particular, they include submarine pillow basalts, submarine jumbled plates, and subaerial ropy and sheet pahoehoe flows.

The effect of a sloping base shifts the regime transitions to smaller values of Ψ (Gregg & Fink 1999) and leads to a flow elongated down slope (Figure 6). The down-slope flow can be channelized by solidified edges in the levee and surface folding regimes, and it can form covered lava tubes at smaller Ψ (discussed further in Section 6.3). An identical sequence of flow regimes was found for PEG flows spreading from a line source (after allowing for appropriate redefinition of Ψ in terms of the flow rate per unit length of the vent; Fink & Griffiths

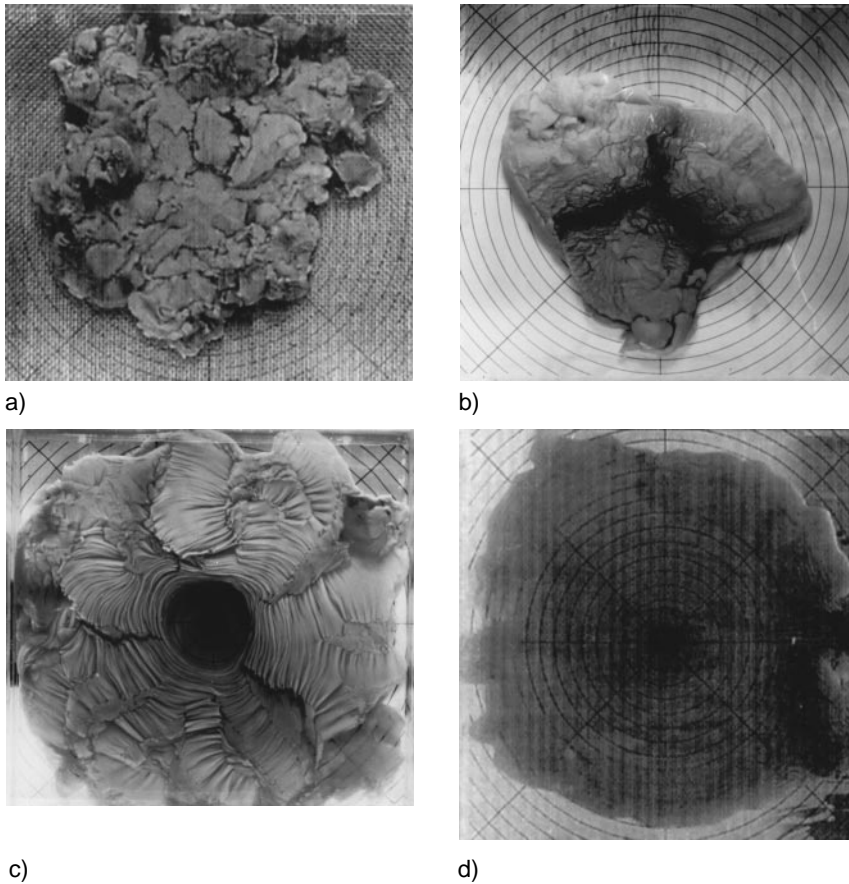


Figure 5 Examples of solidifying gravity currents showing four flow types in laboratory experiments with polyethylene glycol wax flowing over a horizontal floor. The Newtonian liquid was extruded from a small hole onto the base of a tank of cold water. Some of the surface subsequently solidified. (a) Pillow growth at $\Psi = 0.11$; (b) rifting flow with separating rigid surface plates at $\Psi = 2.7$; (c) folded flow at $\Psi = 3.0$; (d) largely axisymmetric flow with solid confined to levees along the flow front at $\Psi = 7.3$ [these values of Ψ have been corrected for a previous numerical mistake; all values reported by Fink & Griffiths (1990) must be divided by $10^{2/3}$].

1992). Thus the regimes of behavior are robust. However, experiments with different fluids are needed to test for possible dependence on material properties.

Laboratory experiments have also been carried out with the spreading of a high-temperature corium melt (mainly hafnia, zirconia, silica, and wustite), which is similar to a melt that may be formed if a severe accident in a pressurized-water nuclear reactor leads to melting of the reactor core (Journeau et al 1999). In

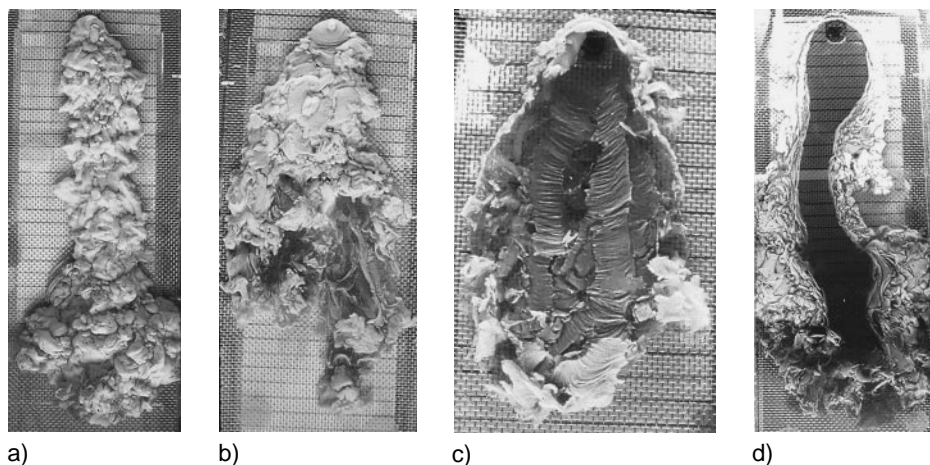


Figure 6 Laboratory experiments with polyethylene glycol wax flowing from a small source on a planar slope under cold water. The base slopes downward to the right and is covered with mesh to make a rough floor. (a) Pillow flow, (b) rifting flow, (c) folded flow, (d) leveed flow. (The tank is 30 cm wide; from Gregg & Fink 1999.) (c) and (d) are similar to ropy pahoehoe and long channelized flows observed in Hawaiian lava flows.

experiments designed to investigate the flow of corium over the floor of the reactor vessel, 17 kg of melt at 2200 K were released to flow under air. The surface of the material cooled by radiation and solidified rapidly, producing a thin thermal and rheological boundary layer. Folding produced a surface appearance similar to ropy pahoehoe lava, all the way from the flow margin to the source. The flow front stopped spreading after ~ 8 s. Unfortunately, values of Ψ cannot be obtained because surface cooling (by 300 K) had taken place before the melt left the source.

Experiments similar to the wax studies above but with a kaolin-PEG slurry, which has both a yield strength and the freezing temperature of the PEG, reveal a different sequence of morphologies (Figure 7). Hence the rheology of the interior fluid plays a role in controlling the forms of flow and deformation, even though the rate of solidification, expressed in Ψ_B , again determined which of the morphologies occurred. At $\Psi_B > 15$ (fast extrusion and slow cooling), the slurry spread axisymmetrically almost as if there were no cooling; at $0.9 < \Psi_B < 15$, there were strong rigid plates over most of the surface and later upward extrusion of ridges with smooth striated sides; at $0.12 < \Psi_B < 0.9$, the flow commenced as a set of four to six (most often five) radially moving lobes having a weak tendency to spiral. Under rapid cooling or very slow effusion, $\Psi_B < 0.12$, the lobes were more like vertical spines and were extruded upward from the vicinity of the source. In these experiments the transitions between regimes were more gradual than those for the viscous fluid. The morphologies strongly resemble

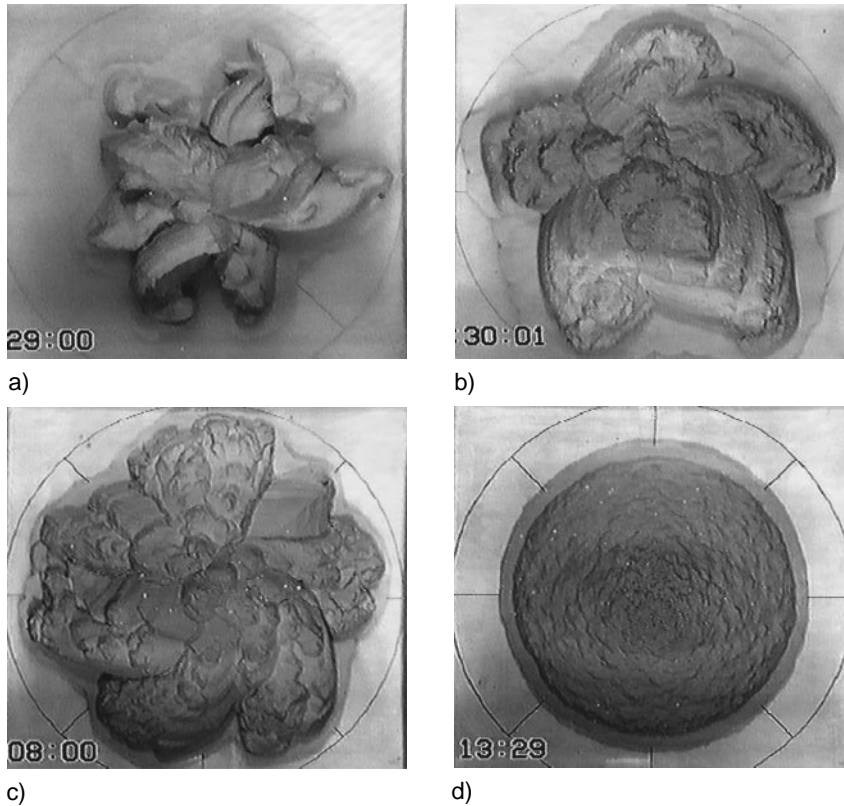


Figure 7 Solidifying flows of a Bingham fluid using a slurry of kaolin in polyethylene glycol. Apart from the fluid rheology, the experiments were similar to those of Figure 6. (a) A spiny extrusion at $\Psi_B = 0.09$, (b) a lobate extrusion showing a typical 5-lobe pattern at $\Psi_B = 0.79$, (c) a flow without distinct lobes but surfaced by solid plates with curving segments, $\Psi_B = 1.3$, (d) an axisymmetric flow almost unaffected by cooling at $\Psi_B = 30$. (Heaviest grid lines are 5 cm apart; from Fink & Griffiths 1998.)

qualitative characteristics of many highly silicic lava domes (Fink & Griffiths 1998).

There has been no adequate theoretical description of the above cooling and solidifying flows or of the various instabilities that lead to asymmetric spreading and irregular structure. Only a gravitational instability in a density-stratified lava dome (Fink 1980b) and the surface buckling instability (Fink & Fletcher 1978, Fink 1980a) have been analyzed. There is good quantitative agreement between the wavelengths of observed folds (on ropy pahoehoe and the laboratory wax flows) and that predicted for the buckling of layers of differing viscosity or yield strength subjected to a compressive stress (Biot 1961).

Scaling relationships for the growth of solidifying flows in several dynamical regimes have been proposed based on a simplified two-component description (Griffiths & Fink 1993). The flow is reduced to an isothermal and rheologically uniform interior (viscous or plastic) and a thin surface layer having different rheological properties—a larger viscosity or yield strength (Figure 8). The surface layer is viewed as largely solidified material (because the solid gives to the greatest rheological difference), and, therefore, it begins at a distance of $\sim d_s$ from the vent if the advection is fast enough, or it may completely encompass the flow if the volume flux is small. In addition, the surface layer thickness δ on each element of surface is assumed to increase approximately as $\delta \sim (\kappa t)^{1/2}$, which translates to a changing thickness $\delta(r)$ with distance from the vent and an increasing crust thickness $\delta_f(t)$ at the flow front. Observation shows that the crust is highly fractured and blocky and therefore is modeled as viscoplastic, with most of its influence on the flow arising from the thickest crust at the flow front. The flow is driven by gravity (integrated force $F_B \sim \rho g H^2 R$) or overpressure (a pressure P_0 in excess of the hydrostatic, giving $F_P \sim P_0 R^2$) and is retarded by both basal stress ($F_\eta \sim \eta \dot{\epsilon} R^2$ if Newtonian, $F_\sigma \sim \sigma_0 R^2$ if plastic) and crustal stresses ($F_{\eta_c} \sim \eta_c \dot{\epsilon} R \delta_f$ for a viscous crust and $F_{\sigma_c} \sim \sigma_c R \delta_f$ for a plastic crust). The usual geometric relation $V \sim R^2 H$ is used to express continuity under the assumption of self-similarity while a flow is within a given regime. Volume is assumed to

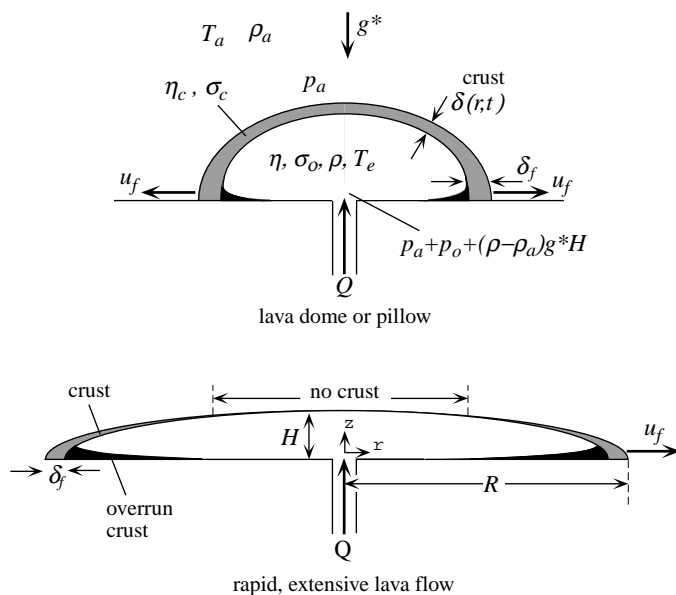


Figure 8 A two-component model for cooling lava flows at small Re . Scaling analysis of the force balances in this model provides predictions for the spreading of flows from point and line sources (Griffiths & Fink 1993, 1997).

increase as $V \sim St^\alpha$. From these scalings, solutions can be found for various crust-controlled asymptotic regimes, extending the previous solutions for homogeneous flows to cases in which the dominant balance is between buoyancy and crust viscosity, buoyancy and crust yield strength, or overpressure and any of the crustal or interior retarding forces. The conditions for transitions between regimes during flow can also be found.

The balance of buoyancy with the yield strength of the crust gives

$$R \sim (\sigma_c/\rho g)^{-1/4} \kappa^{-1/8} S^{1/2} t^{(4\alpha-1)/8}, \quad H \sim [(\sigma_c/\rho g)^{2\alpha} \kappa^\alpha S^{-1} R^2]^{1/(4\alpha-1)}, \quad (20a)$$

and

$$H \sim (\sigma_c/\rho g)^{1/2} (\kappa t)^{1/4}. \quad (20b)$$

In both this model and the uniform plastic flow (Equation 12), the height increases with time. This contrasts with a dominant viscous crust or viscous interior (Equation 8), for which the height is constant (for constant volume flux) or decreases (for $\alpha < 1$). Of greater interest is the result that the flow height in Equation 20b is independent of both internal properties (η and σ_0) and source flux (S and α), whereas, for constant-volume fluxes, isothermal viscous flows have a height increasing with volume flux: $H \sim Q^{1/4}$ (Equation 8), and isothermal plastic domes have $H \sim (Qt)^{1/5}$ (Equation 12), where $Q = S(\alpha = 1)$. The absence of Q in Equation 20b follows from the fact that a smaller-volume flux allows greater time for cooling and formation of thicker crust, which inhibits lateral flow more and gives a flow depth as great as that for larger-volume fluxes. This important result is also illustrated by the variation of height H with overall radius R ; for various models with $\alpha = 1$, isothermal viscous flow has $H \sim Q^{1/4}$ (Equation 8), viscous crust control gives $H \sim Q^{1/7}$, both independent of R (Griffiths & Fink 1993), whereas crust strength control gives the inverse variation with volume flux $H \sim Q^{-1/3} R^{2/3}$ (Equation 20a). Thus a larger-volume flux creates a deeper flow for the purely viscous case but a shallower flow for a strong crust. The difference is again the result of a shorter time available for cooling at larger-volume flux, which implies a thinner crust and less inhibition of spreading. Likewise, slower cooling gives a smaller flow depth.

The experiments of Griffiths & Fink (1993) confirmed this behavior for solidifying wax flows (Figure 9a), the results being consistent with the viscous solutions for $\Psi > 20$ (where there is little or no solid crust), but consistent with the opposite trend (Equation 20a) for $\Psi < 6$ (where crust is obvious). Similarly, the experiments with slurries confirmed that Equation 20 applied to solidifying flows having an interior yield stress (Figure 9b), despite the different morphologies. Other experimental results with corn syrup spreading under cold water, in which cooling produced an increase in viscosity but no solidification or yield strength (Stasiuk et al 1993), have been analyzed in terms of a single value of an apparent (bulk) flow viscosity η_b over the period of observation of the spreading flow (for which the thermal boundary layer was thin). This is in effect a time-averaged form of the flow viscosity η_F defined in Section 3 and, as in Huppert et al (1982),

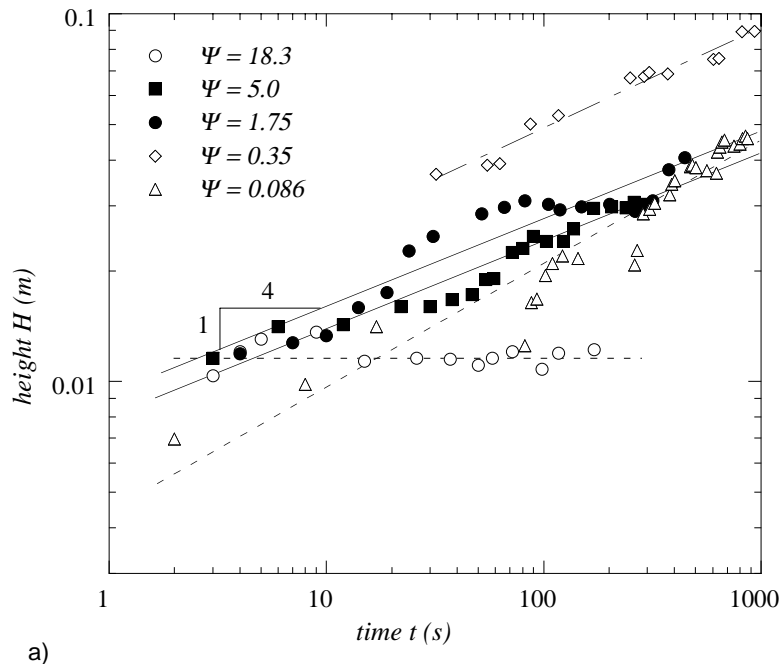


Figure 9 Data for the growth of dome height with time in (a) experiments with solidifying polyethylene glycol (PEG) wax and a source of constant volume flux (Griffiths & Fink 1993), (b) experiments with solidifying kaolin/PEG slurry having a yield stress, solidification temperature of 17°C, and constant volume flux (Griffiths & Fink 1997), (c) four lava domes that grew on La Soufrière (St. Vincent, 1979), Mt. St. Helens (USA, 1981–1986), Mt. Pinatubo (Philippines, 1991), and Mt. Unzen (Japan, 1991–1995). In (a) an experiment with no cooling is included (the run having constant H), the run at the smallest Ψ shows effects of overpressure (*broken line*, $H \sim t^{1/3}$) and the run having $\Psi = 0.35$ gives $H \sim t^{0.27}$. *Solid lines* have slope 1/4. Variability tends to be large under the intermediate conditions. In (b) the flow with largest Ψ_B had solid only at its margins; that with smallest Ψ_B was encapsulated in thick solid and grew through upward spines. The height in these experiments had a trend consistent with the 1/4-power, but there was unexplained scatter in the absolute height and radius at small Ψ_B (possible causes include solid strengths differing between batches of slurry or with ambient water temperatures and the effects of instabilities). In (c) data for the Unzen dome were supplied by S. Nakada and are presented here for the first time—they lie slightly above the straight line fitted previously to the Soufrière and Mt. St. Helens data; data for the other domes are from Fink & Griffiths (1998). The height shown for the Unzen dome, which grew on a slope, is the difference between the highest and lowest reaches of the dome. The four lava domes, the laboratory Bingham domes, and flows of viscous wax having a moderate spreading rate ($0.2 < \Psi < 6$) all evolved in a way consistent with Equation 20b in the text.

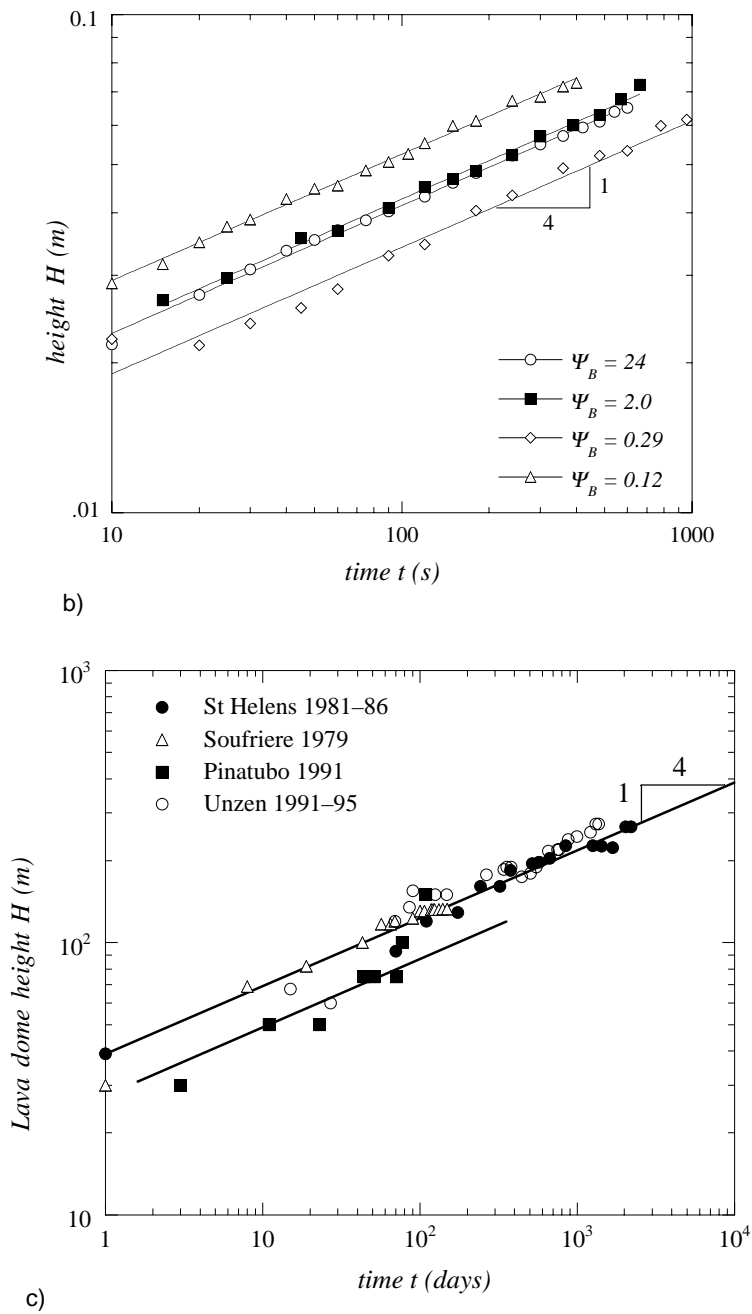


Figure 9 Continued

was defined as the viscosity necessary to fit the form (Equation 8) to the measured $R(t)$. This global viscosity coefficient was found to depend on Pe and the ratio of η_c/η_e , η_e being the viscosity at the vent. The result was shown to be consistent with the similarity solution for flow with a cooling viscous boundary layer and the simpler relation $\eta_B \sim \eta_e Pe^{-4/7}$ (Lister & Kerr 1994).

Comparison of the theoretical scaling with the few available measurements for active lava domes is very useful. Data from four lava domes (the La Soufrière dome of 1979, the Mt. St. Helens dome of 1981–1986, the Mt. Pinatubo dome of 1991, and the Mt. Unzen dome of 1991–1995) give the heights, widths, and volumes as functions of time. These can be used to evaluate the exponent α in each case from the volume estimates (Huppert et al 1982, Griffiths & Fink 1993, Fink & Griffiths 1998). The data from Mt. Unzen, whose lobate dome eruption was described by Nakada & Fujii (1993), is presented here for the first time. For the values of α so obtained, the predicted trends of dome radius with time given by the various models are not greatly different. However, the models of spreading controlled by the yield strength of a developing crust compare most favorably with the data. The predicted trends for dome height with time (or radius) in the various asymptotic regimes are more clearly different and allow a more definite conclusion about which of the models best describes the data. For flow dominated by basal viscous stresses we predict a height decrease with time in each case (except for the first 20 days of growth of the Soufrière dome), whereas the measured dome heights increased (Figure 9c). Hence the viscous models are discounted (unless the crust near the flow front is characterized by an apparent viscosity that increases with time). On the other hand, the model of flow controlled by crustal yield strength is in good agreement with the data, and the best agreement is with the buoyancy-crust strength balance: The predicted $H \sim t^{1/4}$ relation provides a reasonable fit for all four lava domes.

Given the good agreement between the scaling analysis and trend of the data in Figure 9c, Equation 20b is readily applied to evaluate the crustal yield strengths for real lava domes, giving $\sigma_c \sim 1.3 \times 10^8$ Pa for Mt. St. Helens ($70 < t < 2200$ days after commencement of dome growth), 1.5×10^8 Pa for Soufrière ($40 < t < 150$ days; Griffiths & Fink 1993), and 0.9×10^8 Pa for the Pinatubo dome (Fink & Griffiths 1998). For Mt. Unzen dome ($15 < t < 1373$ days), we find $\sigma_c \sim 1.6 \times 10^8$ Pa. These four strengths are remarkably similar given the different dome compositions, basal topography, extrusion rates, eruption durations, and dome morphologies. They may therefore reflect a maximum yield strength achieved by a fractured, jumbled carapace of solidified lava relatively close to the ambient atmospheric temperature. Note that the strength estimate does not require measurements sufficient to estimate the dome volume or exponent α .

The internal lava yield stress has also been estimated by applying the isothermal Bingham model (Equation 12) to the first 20 days of growth of the Soufrière dome and measurements of the dimensions of a small lobe that grew (over a period of 160 minutes) on the Mt. St. Helens dome: the values are $\sigma_0 \sim 2.8 \times 10^5$ Pa and 1.1×10^5 Pa, which are similar to the estimate $\sigma_0 \sim 2.6 \times 10^5$ Pa

obtained by applying the same model to the Soufrière dome at times $t > 40$ days (Blake 1990). An independent but less direct estimate of the internal strength of a number of domes is based on classifying each dome by its dominant qualitative morphology and applying the laboratory relationship between morphology and Ψ_B (as illustrated in Figure 7) to evaluate Ψ_B (Fink & Griffiths 1997). The resulting Ψ_B , taken in conjunction with an estimate of the volume flux and the calculated solidification time t_s for each dome, were then used in Equation 19b to obtain σ_0 . For all of the 14 cases considered, $\sigma_0 \sim (0.5-5) \times 10^5$ Pa. The consistency between these different estimates of internal strength lends weight to the hypothesis that the internal yield stress influences the flow instabilities and morphology found in lava domes, whereas the height and overall spreading are controlled by the crust. The estimates also give $\sigma_c/\sigma_0 \sim 10^3$. With this strength a crust thickness as small as $\delta_f > 10^{-3}R$ (e.g. 1 m in 1000 m) is required for the crust strength to dominate.

6.3 Long Lava Flows

Turning to long basalt flows that extend for many kilometers from their vent, the flow behavior again reflects, albeit in ways that remain poorly understood, differing vent fluxes, eruption duration, underlying topography, and whether they flow under air or water (see e.g. Walker 1973, Pinkerton 1987, Pinkerton & Wilson 1994, Keszthelyi & Self 1998, Cashman et al 1998). Field evidence indicates that surface cooling leads to the formation of a glassy crust, whereas internal mixing can cause disruption or entrainment of this crust, cooling, and rheological changes in the interior. Development of side levees removes mass from the advancing flow front and represents formation of a flow-defined channel. In some circumstances, cooling produces such a strong crust that it forms a rigid connected roof beneath which rapid, thermally insulated flow continues in a lava tube. There are so many processes involved that, in past attempts to model these flows, some of them are approximated by empirical parameterizations. A key factor that has proved particularly difficult to model in a predictive manner is the effect of cooling, which depends on the amount and rate of disruption, of cooled surface crust. The disruption of crust has been described in terms of an empirical fraction of the surface representing exposed incandescent fluid from the flow interior. This fraction has been expressed as a function of the mean flow velocity (Crisp & Baloga 1990) but awaits a theoretical model. The aim is again to predict factors such as the rate of cooling with distance downstream, flow thickness, the speed of advance of the flow front, changes in flow regime, and the final length of a flow. Given the complexities of long lava flows, simple theoretical results and complex parameterized computational models are both valuable. Arguably, they lend more understanding than do computational simulations with primitive equations but finite spatial resolution. However, there is a need to remove empirical approximations from models, replacing them with parameterizations based on testable and predictive physical models of the relevant processes.

Many of the processes and studies mentioned above in the context of creeping flows are equally relevant to long flows, so long as these are slow, as for a shallow breakouts from the main channel or flow front. Most models of large basalt flows, on the other hand, have taken a different approach and assumed vertically uniform temperature within the flow, in some cases including a thin crust that offers thermal insulation and appears in the model heat equation but has no mechanical influence in the momentum equations (Dragoni 1989; Dragoni & Tallarico 1994; Crisp & Baloga 1990, 1994). They also assume flow down a prescribed channel.

For a thermally mixed flow having no temperature or velocity variations with depth, a control-volume formulation for the local temperature $T(x,t)$ gives

$$DT/Dt = (L/c_p)d\phi/dt - F_s/\rho c_p h, \quad (21)$$

where $h(x, t)$ is the local flow depth. The rate of latent heat release is small (generally $<1\%$ of the surface flux). The surface heat loss F_s is largely radiative, discussed in Section 4, and has been expressed in terms of the internal temperature T (as opposed to the surface temperature T_e) as $F_s = e\Sigma f T^4$, where f is an effective fraction of the surface over which high-temperature incandescent lava is exposed (Crisp & Baloga 1990). Hence the characteristic timescale for cooling is $\Gamma = (\rho c_p H)/(e\Sigma f T_e^3)$. If we further assume no variation in along-stream velocity U and a constant mass flux q per unit width (e.g. Danes 1972, Park & Iverson 1984), Equation 21 reduces to the simple form

$$c_p q dT/dx + e\Sigma f T^4 = 0, \quad (22)$$

which has the solution $T(x)/T_e = [(3/UG)x + 1]^{-1/3}$, or $T \sim x^{-1/3}$ at large x . The timescale Γ (with $f = 1$) is on the order of 1 day (Crisp & Baloga 1990), whereas observed flow emplacement times are only 1- to 10-fold longer. This comparison is evidence that Γ is a relevant timescale and that emplacement times are limited by cooling rather than vent supply duration. Observed values of f (~ 0.001 – 0.1) imply larger values of Γ . However, the temperature need only decrease from $T_e \approx 1150^\circ\text{C}$ to $\sim 1100^\circ\text{C}$ before the crystallinity reaches the critical value of $\sim 45\%$ for onset of a yield strength and $\sim 50\%$ – 60% for cessation of flow. This amount of cooling requires only a small fraction of the time Γ . A more detailed thermal model allows for heat loss from the low-temperature crust covering a fraction $1 - f$ of the surface (Crisp & Baloga 1990) and conductive cooling at the base. In the limit $f = 0$, the flow interior is completely insulated by a conductive crust, and Γ is replaced by a much longer timescale based on the heat flux from a relatively low surface temperature.

Thermal models have been linked to the dynamic by assuming steady, hydrostatic, two-dimensional motion (i.e. a prescribed channel of uniform width and slope, with no cross-channel variations) and neglecting the pressure gradients owing to the gradient of flow depth dh/dx relative to those caused by the topographic slope β (i.e. $H/L \ll \sin\beta$). The application of a Bingham flow law to motion along the down-slope channel yields (e.g. Dragoni 1989)

$$u(x, z) = [(\rho g \sin \beta) / 2 \eta] z(2h - z) - 2\sigma_0 z, \quad 0 < z < h - h_s$$

$$[(\rho g \sin \beta) / 2 \eta] h^2 (1 - \sigma_0 / \sigma_b)^2, \quad h - h_s < z < h, \quad (23)$$

where $\eta(x)$ is the plastic viscosity as before, $\sigma_b(x) = \rho g h \sin \beta$ is the shear stress at the base of the flow, and $h_s(x)$ is the critical depth (14). The latter represents the thickness of the undeformed plug at the top of the flow, in which the shear stress is less than $\sigma_0(x)$. Expressions such as Equations 2 and 3 relate the viscosity and yield strength to temperature and crystallinity (Park & Iverson 1984, Dragoni 1989). Cooling causes the apparent viscosity $\eta_a = \eta + \sigma_0 / \dot{\epsilon}$ to increase downstream, in turn causing the velocity to decrease and the flow to deepen with distance downstream. The model flows attain a very large apparent viscosity (especially with the onset of a yield strength) at some distance from the vent and effectively come to a halt with a very large flow thickness. The flow depth near the vent is greater than h_s but eventually becomes equal to h_s as the critical depth increases downstream. Comparison with sparse available data from lava flows shows qualitative agreement, with flows cooling and slowing at distances 10^2 to 10^4 m from the vent, and predicted advection times of hours to days for realistic volume fluxes and rheological parameter values. The behavior, particularly the flow depth downstream, is very sensitive to volume flux. As found in the scaling for laminar flows, the flow thickness can be larger for smaller-volume fluxes, a consequence of the effects of smaller advection velocity relative to the rate of cooling. The results are also sensitive to the assumption of either efficient vertical mixing or thermal stratification (Dragoni 1989).

Although the available models capture the gross features of long channelized flows, there are many factors yet to be included. The control-volume formulations are not time-dependent, so they do not indicate that subsequent volumes from a steady eruption come to a halt at different distances from the vent, and changes in eruption rate are not allowed for. Hence these models do not allow a full investigation of flow front advance or of the effect of cooling relative to the effect of erupted volume. The thin flow approximation also cannot capture processes occurring near the flow margins, where the depth variation $dh/dx > \sin \beta$. Importantly, long cooling flows without a prescribed channel have not received much theoretical attention. In this case flow may spread across slope, form levees, or branch (as in numerical experiments with complex distributary systems; Miyamoto & Sasaki 1998).

Excellent qualitative results relevant to long lava flows are obtained from the laboratory analog experiments already discussed in Section 6.2 for cooling flows on a horizontal base (Fink & Griffiths 1990, 1992; Griffiths & Fink 1997) and on planar slopes (Hallworth et al 1987, Gregg & Fink 1999). Results obtained with freezing PEG wax on a slope (Figure 6) show that four characteristic regimes occur, as on a horizontal base, but with down-slope elongation and channelization. The regimes again appear to be delineated by ranges of the dimensionless solidification time (or advection speed) Ψ , with an added dependence on slope angle.

In these experiments the solidifying flow determines its own channel width, the width may vary with distance downstream and with time, and the mass flux decreases with distance down the channel as a result of continuous levee building, branching, or roof construction. These are laminar flows. Conditions for the disruption and mixing of surface crust under stresses imposed by the underlying flow and conditions for stable crust are not known for either laminar or turbulent flows, yet they determine the distance down channel at which vertically mixed flow gives way to the onset of a thickening surface layer and stratified flow (Kilburn 1993, Cashman et al 1999b). Also remaining unpredicted are the mechanical and thermal conditions required for formation of lava tubes (e.g. Peterson et al 1994, Kauahikaua et al 1998).

6.4 Flows With Melting of the Base

Thermal erosion caused by melting of underlying sediments or rock by basaltic lava flows has been investigated as the cause of sinuous rilles observed on the moon (Hulme 1973, 1982). Similar erosion by much hotter ($>1400^{\circ}\text{C}$) and very low-viscosity (0.1- to 10-Pa) komatiite lavas has been invoked to explain channels and embayments beneath terrestrial komatiite flows. Rich Fe-Ni-Cu sulfide deposits are found at the foot of the latter embayments and are thought to have formed by thermal erosion of sulfur-rich rocks by metal-rich lavas, followed by the segregation and accumulation of dense immiscible metal sulfide melts (Leshner & Campbell 1993). Theoretical modeling by Huppert et al (1984), Huppert & Sparks (1985), and Turner et al (1986) has suggested that komatiites erupted and flowed for large distances as turbulent currents, had high cooling rates under seawater, and could have produced thermal erosion 10–100 km from their sources. The extent of melting may have led to significant contamination of the flow by the assimilated melt. Huppert (1989) analyzed the time-dependence to show that there will always be some initial solidification at the cool boundary (if T_s is greater than the initial boundary temperature), followed by a remelting phase and then melting of the original boundary (if the flow is hotter than the boundary melting temperature). The geometry of erosion channels has been addressed by Jarvis (1995) and predicted to involve undercutting of the edges. Mathematical modeling by Williams et al (1998) indicates that erosion is strongly dependent on the nature of the base material, with hydrous sediment being fluidized by vaporized seawater and strongly eroded, whereas relatively little erosion is predicted to occur for consolidated anhydrous sediment.

The modeling involves solution of a heat equation similar to Equation 21 but having two additional terms to account for the turbulent heat flux to the base and the heat required to raise melted substrate to the lava temperature. The surface flux term is replaced by the turbulent flux at the bottom of a solid crust, where the steady-state crust temperature is given by an independent relation equating the turbulent heat flux into the crust from the interior lava to the surface heat loss through buoyancy-driven convection in the overlying water. The steady-state

crust thickness is then found by equating the conductive flux through the crust to the convective flux into the water. The crust provides good insulation to the flowing lava. The steady-state thermal erosion rate u_m into the substrate is given by equating heat fluxes at the melting interface:

$$u_m = C_T(T - T_m)/E_m, \quad (24)$$

where C_T is the turbulent heat transfer coefficient in the lava, T is the lava temperature, T_m is the melting temperature of the ground, and E_m is the energy (per unit volume) required to melt the ground. The flow velocity in this two-dimensional control-volume formulation for moderate to large Re is simply $u = 2[g/h\sin\beta/C_D]^{1/2}$, where g is the reduced gravity and C_D (Re) is a suitable friction coefficient.

The calculations indicate that a submarine komatiite lava, erupted at its liquidus temperature and initially 10 m thick, could have flowed hundreds of kilometers from its source, a result consistent with field observations. If the eruption durations were <2 weeks, only small extents of thermal erosion (on the order of meters) are likely to have occurred (Williams et al 1998). However, this model is based on the questionable assumption that a solid crust is able to form at the lava-water interface despite agitation by the underlying turbulent flow. No models have taken into account the potentially large effects on heat transfer of a more viscous melt boundary layer or morphological instabilities on the melting boundary, and the value of the heat transfer coefficient from the lava to the base is very uncertain owing to a number of such boundary-related effects. The model could potentially be applied to the somewhat cooler basaltic sheet flows that are found to be ~ 100 km long on the present sea floor and to submarine flood basalt flows. On land, the cooler and much smaller flows of channelized basalt on Hawaii show clear evidence for thermal erosion by melting of the underlying rocks (Kauahikaua et al 1998). On the other hand, field observations of long flows indicate that well-insulated flow in lava tubes or inflated sheets capped by crust provides a mechanism for long-distance travel of small-to-moderate volume fluxes without significant cooling. This appears to rule out the requirement of very high eruption rates previously postulated for flood basalts and calls into question the occurrence of fully turbulent flows (Cashman et al 1998). The field observations (e.g. Kauahikaua et al 1998) also highlight the need for models of flows at transitional Reynolds numbers and transitional thermal regimes.

7. CONCLUSIONS

The dynamics of lava flows pose many challenges. In detail they are complex in thermodynamics and rheology and therefore in mechanics. An interdisciplinary approach is beneficial to identify the critical processes in the light of both field observations (which I have not attempted to review here) and theoretical fluid mechanics, to formulate physically consistent models, and to compare solutions

with available data. Theoretical solutions have been given for simple isothermal flows and have been tested by using well-controlled laboratory experiments. They provide explanations of the most elementary characteristics of lava flows, and demonstrate some of the implications of viscous and Bingham flow. However, the real value of these solutions is that they serve as a basis of comparison for more complex models, allowing a greater understanding of the effects of additional factors or processes. In particular, since lavas are erupted at temperatures of 900°–1200°C above those of their new environment but <200°C above their solidus, it is not surprising that the effects of heat loss are large. The thermal effects and consequent rheological change influence the overall flow depth and average spreading rate. The onset of a yield strength in cooled portions of the flow is inevitable after sufficient crystallization has occurred, and this is generally responsible for eventually halting the advance of the flow front. Thermal effects also lead to a range of complexity, including rheologically heterogeneous flows and instabilities such as flow branching and the formation of surface folds, solidified plates or blocks, submarine pillows, creases, flow lobes, spines, and extrusion surfaces. Laboratory analog experiments have been invaluable in relating these instabilities and other characteristics of flows to flow conditions, especially the vent volume flux, cooling rate, base slope, and the effects of a yield strength. Scaling analyses too have been useful for these more complex flows. However, many processes remain poorly understood and lack a theoretical description.

Theoretical and computational developments must overcome the difficulties introduced by a moving free surface that is also the boundary at which the thermal and rheological changes tend to be strongly concentrated and where flow instabilities arise. However, new computational approaches may soon provide insight into instabilities such as flow branching (e.g. Miyamoto & Sasaki 1998). There are opportunities also for new theoretical formulations and laboratory experiments designed to investigate the temporal evolution of long flows in a prescribed channel, the processes controlling the width of flow-generated channels and the consequent rate of flow front advance, the stability of a surface crust to disruption by underlying stresses (to predict heat loss, and crust growth), the entrainment of crust into the bulk of the underlying flow (to predict interior cooling), the conditions required for formation of lava tubes, better descriptions of the thermal and rheological evolution of growing lava domes, and the nature of the lobate instability in cooling Bingham flows. Much has yet to be understood about the hazard potential of lava domes on steep slopes, where flow front collapse can produce a destructive pyroclastic flow. The effects of bubbles on rheology require further attention, as do the flow dynamics of cooling, highly vesiculated lava (i.e. flow of foams) and the role of volatile pressure in flow front stability.

ACKNOWLEDGMENTS

I thank Jonathan Fink and Katharine Cashman for introducing me to the fascinations of volcanology and for their patience when posing difficult fluid dynamical questions that I could not always answer. I thank them also, along with Ross

Kerr and David Osmond, for valuable comments on a draft of this review and for kindly providing photographs.

Visit the Annual Reviews home page at www.AnnualReviews.org.

LITERATURE CITED

- Anderson SW, Fink JH. 1990. The development and distribution of surface textures at the Mount St. Helens dome. See Fink 1990, pp. 25–46
- Balmforth NJ, Burbidge AS, Craster RV, Salzig J, Shen A. 1999. Visco-plastic models of isothermal lava domes. *J. Fluid Mech.* In press
- Balmforth NJ, Craster RV. 1999. A consistent thin-layer theory for Bingham fluids. *J. Non-Newtonian Fluid Mech.* 84. In press
- Biot MA. 1961. Theory of folding of stratified visco-elastic media and its implications in tectonics and orogenesis. *Bull. Geol. Soc. Am.* 72:1595–620
- Blake S. 1990. Visco-plastic models of lava domes. See Fink 1990, pp. 88–128
- Cashman KV, Pinkerton H, Stephenson PJ. 1998. Long lava flows. *J. Geophys. Res.* 103:27281–89
- Cashman KV, Sturtevant B, Papale P, Navon O. 1999a. Magmatic fragmentation. In *Encyclopedia of Volcanology*. New York: Academic. In press
- Cashman KV, Thornber CR, Kauahikaua JP. 1999b. Cooling and crystallization of lava in open channels, and the transition of pahoehoe lava to `a`a. *Bull. Volcanol.* In press
- Crisp J, Baloga S. 1990. A model for lava flows with two thermal components. *J. Geophys. Res.* 95:1255–70
- Crisp J, Baloga S. 1994. Influence of crystallisation and entrainment of cooler material on the emplacement of basaltic `a`a lava flows. *J. Geophys. Res.* 99:11819–32
- Danes ZF. 1972. Dynamics of lava flows. *J. Geophys. Res.* 77:1430–32
- Dragoni M. 1989. A dynamical model of lava flows cooling by radiation. *Bull. Volcanol.* 51:88–95
- Dragoni M, Tallarico A. 1994. The effect of crystallisation on the rheology and dynamics of lava flows. *J. Volcanol. Geotherm. Res.* 59:241–52
- Fink JH. 1980a. Surface folding and viscosity of rhyolite flows. *Geology* 8:250–54
- Fink JH. 1980b. Gravity instability in the Holocene and Little Glass Mountain rhyolite obsidian flows, northern California. *Tectonophysics* 66:147–66
- Fink JH, ed. 1990. *Lava Flows and Domes: Emplacement Mechanisms and Hazard Implications*. IAVCEI Proc. Volcanol., Vol. 2. Springer-Verlag, New York, IUGG Congress, Vancouver, B.C., 249 pp.
- Fink JH, Fletcher RC. 1978. Ropy pahoehoe: surface folding of a viscous fluid. *J. Volcanol. Geotherm. Res.* 4:151–70
- Fink JH, Griffiths RW. 1990. Radial spreading of viscous-gravity currents with solidifying crust. *J. Fluid Mech.* 221:485–510
- Fink JH, Griffiths RW. 1992. A laboratory analog study of the morphology of lava flows extruded from point and line sources. *J. Volcanol. Geotherm. Res.* 54:19–32
- Fink JH, Griffiths RW. 1998. Morphology, eruption rates and rheology of lava domes: insights from laboratory models. *J. Geophys. Res.* 103:527–46
- Fink JH, Malin MC, Anderson SW. 1990. Intrusive and extrusive growth of the Mount St. Helens lava dome. *Nature* 348:435–37
- Gregg TKP, Fink JH. 1999. A laboratory investigation into the effects of slope on lava flow morphology. *J. Volcanol. Geotherm. Res.* In press
- Griffiths RW, Fink JH. 1992a. The morphology of lava flows under planetary environments:

- predictions from analog experiments. *J. Geophys. Res.* 97:19739–48
- Griffiths RW, Fink JH. 1992b. Solidification and morphology of submarine lavas: a dependence on extrusion rate. *J. Geophys. Res.* 97:19729–37
- Griffiths RW, Fink JH. 1993. Effects of surface cooling on the spreading of lava flows and domes. *J. Fluid Mech.* 252:667–702
- Griffiths RW, Fink JH. 1997. Solidifying Bingham extrusions: a model for the growth of silicic lava domes. *J. Fluid Mech.* 347:13–36
- Hallworth MA, Huppert HE, Sparks RSJ. 1987. A laboratory simulation of basaltic lava flows. *Mod. Geol.* 11:93–107
- Huang X, Garcia MH. 1998. A Herschel-Bulkley model for mud flow down a slope. *J. Fluid Mech.* 374:305–33
- Hulme G. 1973. Turbulent lava flow and the formation of lunar sinuous rilles. *Mod. Geol.* 4:107–17
- Hulme G. 1974. The interpretation of lava flow morphology. *Geophys. J. R. Astr. Soc.* 39:361–83
- Hulme G. 1982. A review of lava flow processes related to the formation of lunar sinuous rilles. *Geophys. Surv.* 5:245–79
- Huppert HE. 1982a. Flow and instability of a viscous current down a slope. *Nature* 300:427–29
- Huppert HE. 1982b. The propagation of two-dimensional and axisymmetric viscous gravity currents over a rigid horizontal surface. *J. Fluid Mech.* 121:43–58
- Huppert HE. 1989. Phase changes following the initiation of a hot turbulent flow over a cold solid surface. *J. Fluid Mech.* 198:293–319
- Huppert HE, Shepherd JB, Sigurdsson H, Sparks RSJ. 1982. On lava dome growth, with application to the 1979 lava extrusion of the Soufrière of St Vincent. *J. Volcanol. Geotherm. Res.* 14:199–222
- Huppert HE, Sparks RSJ. 1985. Komatiites. I. Eruption and flow. *J. Petrol.* 26:694–725
- Huppert HE, Sparks RSJ, Turner JS, Arndt NT. 1984. Emplacement and cooling of komatiite lavas. *Nature* 309:19–22
- Iverson RM. 1990. Lava domes modelled as brittle shells that enclose pressurised magma, with application to Mount St. Helens. See Fink 1990, pp. 47–69
- Jarvis RA. 1995. On the cross-sectional geometry of thermal erosion channels formed by turbulent lava flows. *J. Geophys. Res.* 100:10127–40
- Journeau F, Sudreau F, Gatt J-M, Cognet G. 1999. Thermal, physico-chemical and rheological boundary layers in multi-component oxidic melt spreads. *Rev. Gen. Therm.* In press
- Kauahikaua JP, Cashman KV, Mattox TN, Hon K, Heliker CC, et al. 1998. Observations on basaltic lava streams in tubes from Kilauea Volcano, Hawaii. *J. Geophys. Res.* 103:27303–24
- Kerr RC, Lister JR. 1991. The effects of shape on crystal settling and on the rheology of magmas. *J. Geol.* 99:457–67
- Keszthelyi L, Denlinger R. 1996. The initial cooling of pahoehoe flow lobes. *Bull. Volcanol.* 58:5–18
- Keszthelyi L, Self S. 1998. Some physical requirements for the emplacement of long basaltic lava flows. *J. Geophys. Res.* 103:27447–64
- Kilburn CRJ. 1993. Lava crusts, aa flow lengthening and the pahoehoe-aa transition. In *Active Lavas*, ed. CRJ Kilburn. London: UCL. pp. 263–80
- Lejeune A, Richet P. 1995. Rheology of crystal-bearing silicate melts: an experimental study at high viscosities. *J. Geophys. Res.* 100:4215–29
- Leshner CE, Campbell IH. 1993. Geochemical and fluid dynamical modeling of compositional variations in Archean Komatiite-hosted nickel sulfide ores in Western Australia. *Econ. Geol.* 88:804–816
- Leshner CE, Cashman KV, Mayfield JD. 1999. Kinetic controls on the crystallization of Tertiary North Atlantic basalts: implica-

- tions for the emplacement and cooling histories of near-vent lavas at ODP Site 989, SE Greenland rifted margin. In *ODP Sci. Res. Leg 163 Scientific Results*. In press
- Lister JR. 1992. Viscous flows down an inclined plane from point and line sources. *J. Fluid Mech.* 242:631–53
- Lister JR, Kerr RC. 1989. The propagation of two-dimensional and axisymmetric gravity currents along a fluid interface. *J. Fluid Mech.* 203:215–49
- Lister JR, Kerr RC. 1994. Influence of cooling on lava-flow dynamics: comment. *Geology* 22:93–94
- Manga M, Stone HA. 1994. Interactions between bubbles in magmas and lavas: effects of bubble deformation. *J. Volcanol. Geotherm. Res.* 63:267–79
- Manga M, Castro J, Cashman KV, Loewenberg M. 1998. Rheology of bubble-bearing magmas: theoretical results. *J. Volcanol. Geotherm. Res.* 87:15–28
- Marsh BD. 1981. On the crystallinity, probability of occurrence, and rheology of lava and magma. *Contrib. Mineral. Petrol.* 78:85–98
- McBirney AR, Murase T. 1984. Rheological properties of magmas. *Annu. Rev. Earth Sci.* 12:337–57
- Moore JG. 1975. Mechanism of formation of pillow lava. *Am. Sci.* 63:269–77
- Miyamoto H, Sasaki S. 1998. Numerical simulations of lava flows: roles of parameters on lava flow morphologies. *J. Geophys. Res.* 103:27489–502
- Murase T, McBirney AR. 1973. Properties of some common igneous rocks and their melts at high temperatures. *Geol. Soc. Am. Bull.* 84:3563–92
- Nakada S, Fujii T. 1993. Preliminary report on the activity at Unzen Volcano (Japan) November 1990–November 1991: dacite lava domes and pyroclastic flows. *J. Volcanol. Geotherm. Res.* 54:319–33
- Neri A. 1998. A local heat transfer analysis of lava cooling in the atmosphere: application to thermal diffusion-dominated lava flows. *J. Volcanol. Geotherm. Res.* 81:215–43
- Nguyen QD, Boger DV. 1992. Measuring the properties of yield stress fluids. *Annu. Rev. Fluid Mech.* 24:47–88
- Nye JF. 1952. Mechanics of glacier flow. *J. Glaciol.* 2:82–93
- Osmond DI, Griffiths RW. 1998. Silicic lava domes on slopes. In *Proc. 13th Australasian Fluid Mech. Conf.*, ed. MC Thomson, K Hourigan, Monash Univ., Melbourne, pp. 827–30. Monash Univ., Melbourne, Australia.
- Park S, Iverson JD. 1984. Dynamics of lava flow: thickness growth characteristics of steady two-dimensional flow. *Geophys. Res. Lett.* 11:641–44
- Peterson DW, Holcomb RT, Tilling RI, Christiansen RL. 1994. Development of lava tubes in the light of observations at Mauna Ulu, Kilauea Volcano, Hawaii. *Bull. Volcanol.* 56:343–60
- Pinkerton H. 1987. Factors affecting the morphology of lava flows. *Endeavour* 11:73–79
- Pinkerton H, Sparks RSJ. 1978. Field measurements of the rheology of lava. *Nature* 276:383–85
- Pinkerton H, Stevenson RJ. 1992. Methods of determining the rheological properties of magmas at sub-liquidus temperatures. *J. Volcanol. Geotherm. Res.* 53:47–66
- Pinkerton H, Wilson L. 1994. Factors controlling the length of channel-fed lava flows. *Bull. Volcanol.* 56:108–20
- Roscoe R. 1952. The viscosity of suspensions of rigid spheres. *Br. J. Appl. Phys.* 3:267–69
- Roscoe R. 1953. Suspensions. In *Flow Properties of Disperse Systems*, ed. JJ Hermans, pp. 1–38. New York: North Holland
- Shaw HR. 1969. Rheology of basalt in the melting range. *J. Petrol.* 10:510–35
- Shaw HR, Wright TL, Peck DL, Okamura R. 1968. The viscosity of basaltic magma: an analysis of field measurements in Maka-

- opuhi lava lake, Hawaii. *Am. J. Sci.* 266:255–64
- Smith JV. 1997. Shear thickening dilatancy in crystal-rich flows. *J. Volcanol. Geotherm. Res.* 79:1–8
- Skelland AHP. 1967. *Non-Newtonian Flow and Heat Transfer*. New York: Wiley. 469 pp.
- Stasiuk MV, Jaupart C, Sparks RSJ. 1993. Influence of cooling on lava-flow dynamics. *Geology* 21:335–38
- Turner JS, Huppert HE, Sparks RSJ. 1986. Komatiites. II. Experimental and theoretical investigations of post-emplacement cooling and crystallization. *J. Petrol.* 27:397–437
- Walker GPL. 1973. Factors controlling the lengths of lava flows. *Philos. Trans. R. Soc. London Ser. A* 274:107–18
- Williams DA, Kerr RC, Leshner CM. 1998. Emplacement and erosion by Archean komatiite lava flows at Kambalda: revisited. *J. Geophys. Res.* 103:27533–49
- Wilson L, Head JW III. 1983. A comparison of volcanic eruption processes on Earth, Moon, Mars, Io and Venus. *Nature* 302:663–69



CONTENTS

Scale-Invariance and Turbulence Models for Large-Eddy Simulation, <i>Charles Meneveau, Joseph Katz</i>	1
Hydrodynamics of Fishlike Swimming, <i>M. S. Triantafyllou, G. S. Triantafyllou, D. K. P. Yue</i>	33
Mixing and Segregation of Granular Materials, <i>J. M. Ottino, D. V. Khakhar</i>	55
Fluid Mechanics in the Driven Cavity, <i>P. N. Shankar, M. D. Deshpande</i>	93
Active Control of Sound, <i>N. Peake, D. G. Crighton</i>	137
Laboratory Studies of Orographic Effects in Rotating and Stratified Flows, <i>Don L. Boyer, Peter A. Davies</i>	165
Passive Scalars in Turbulent Flows, <i>Z. Warhaft</i>	203
Capillary Effects on Surface Waves, <i>Marc Perlin, William W. Schultz</i>	241
Liquid Jet Instability and Atomization in a Coaxial Gas Stream, <i>J. C. Lasheras, E. J. Hopfinger</i>	275
Shock Wave and Turbulence Interactions, <i>Yiannis Andreopoulos, Juan H. Agui, George Briassulis</i>	309
Flows in Stenotic Vessels, <i>S. A. Berger, L-D. Jou</i>	347
Homogeneous Dynamos in Planetary Cores and in the Laboratory, <i>F. H. Busse</i>	383
Magnetohydrodynamics in Rapidly Rotating spherical Systems, <i>Keke Zhang, Gerald Schubert</i>	409
Sonoluminescence: How Bubbles Turn Sound into Light, <i>S. J. Putterman, K. R. Weninger</i>	445
The Dynamics of Lava Flows, <i>R. W. Griffiths</i>	477
Turbulence in Plant Canopies, <i>John Finnigan</i>	519
Vapor Explosions, <i>Georges Berthoud</i>	573
Fluid Motions in the Presence of Strong Stable Stratification, <i>James J. Riley, Marie-Pascale Lelong</i>	613
The Motion of High-Reynolds-Number Bubbles in Inhomogeneous Flows, <i>J. Magnaudet, I. Eames</i>	659
Recent Developments in Rayleigh-Benard Convection, <i>Eberhard Bodenschatz, Werner Pesch, Guenter Ahlers</i>	709
Flows Induced by Temperature Fields in a Rarefied Gas and their Ghost Effect on the Behavior of a Gas in the Continuum Limit, <i>Yoshio Sone</i>	779